SUPPRESSION OF COMBUSTION OSCILLATIONS

WITH

MECHANICAL DAMPING DEVICES

PHASE II INTERIM REPORT

Written by: G. D. Garrison
Assistant Project Engineer

A. C. Schnell
Senior Experimental Engineer

J. W. Koenig
Experimental Engineer

Approved by: G. D. Garrison
Program Manager

Pratt & Whitney Aircraft

DIVISION OF UNITED AIRCRAFT CORPORATION

UA®

FLORIDA RESEARCH AND DEVELOPMENT CENTER
BOX 2691, WEST PALM BEACH, FLORIDA 33402

ed in the United States of America

FOREWORD

This report describes work completed during the period 27 June 1969 through 26 June 1970 under Phase II of Contract NAS8-21310 for the NASA Marshall Space Flight Center. The NASA Technical Monitor is Mr. R. H. Counts. Dr. Uno Ingard of the Massachusetts Institute of Technology served as technical consultant.

ABSTRACT

As a result of the Phase I effort under Contract NAS8-21310, acoustic liner technology matured to the extent that thrust chamber firings could be used effectively to obtain quantitative acoustic data for verification of liner design theory. Such data were obtained under Phase II of the program during firings of a specially instrumented rocket chamber at nominal test conditions of 100-psia chamber pressure and 1000-lb thrust using N_2O_4 oxidizer and 50% N_2H_4-50% UDMH fuel. The special instrumentation consisted of several small resonator array elements from which pressure-phase data were obtained while the motor was experiencing unstable combustion. From the pressure-phase data, the following were computed: the acoustic resistance, reactance, and absorption coefficients of the resonators, the particle velocities in the resonator apertures, and the incident energy levels under hot-firing conditions. A comparison of the experimental acoustic resistance with the cold-flow-based theory showed satisfactory agreement. Comparison of the acoustic reactance data with results obtained from previous cold-flow experiments did not show good agreement, but a suitable empirical correlation was derived from the hot test data. The experimental absorption coefficients, when compared with values predicted using the present theory, showed an average deviation of only 11%, which led to the conclusion that the theory is satisfactory for use in designing resonator arrays for rocket combustion chambers.

CONTENTS

ILLUSTRATIONS

ILLUSTRATIONS (Continued)

SECTION I
PROGRAM SUMMARY

A. BACKGROUND

The capability of absorbing liners to suppress combustion instabilities in rocket thrust chambers has been substantiated by experiments conducted over a wide range of thrust levels and chamber pressures, and with several propellant combinations. Although not all liner applications have been completely successful, the majority of successful liners have been designed using the analysis techniques and theory developed at Pratt & Whitney Aircraft through the research sponsored by NASA MSFC under Contracts NAS8-11038 and NAS8-21310. The theory is based on the assumptions that the liner acts as an array of Helmholtz resonators and that a measure of the suppression characteristics of the liner can be obtained through the use of an absorption coefficient defined as the ratio of the energy absorbed by the array to the wave energy acting on the surface of the liner. Theoretically, the suppression capability of the liner is maximized when the coefficient is unity.

The design of resonator arrays for usual acoustical applications is a simple and straightforward process. However, many complex factors affect the application of the theory to the design of rocket chamber absorbers. High gas temperatures, complex flow situations, high pressure amplitudes, and other related effects impose serious limitations and uncertainties on the design techniques. In the NASA-sponsored programs, a systematic approach to the solution of these problems has been applied. The effects of each of the above factors on absorption has been quantitatively described and corroborated through cold flow experiments using ambient air and gaseous helium and nitrogen as test media.

Extrapolation of the liner design theory, based on the results of cold-flow experiments, to hot firing conditions introduces significant uncertainties, primarily because the magnitude of pressure oscillations, particle velocities, and gas flows can only be approached in cold-flow simulations. In the past, it had been necessary to assume that the results from the cold-flow experiments would be applicable, principally because there were no known reliable experimental techniques for making similar

measurements during firings. During the first year of work under Contract NAS8-21310, the pressure-phase impedance measuring technique described in Reference 1 was developed for use during actual rocket firings. Under the current program this technique was used to obtain liner impedance data from carefully controlled hot-firing experiments.

B. OBJECTIVE AND APPROACH

The specific objective of the Phase II work reported herein was to verify acoustic liner design assumptions by obtaining hot firing data in experimental rocket tests. To accomplish this, impedance measuring techniques developed during the previous year of effort were adapted for use in a small, dynamically unstable rocket motor.

Specially instrumented small resonator array elements from which pressure-phase data could be obtained were installed in the chamber. The resonator cavities were constructed so that exact cavity impedance formulations could be used in the data reduction process and the motor was designed so that the effects of gas flow past the resonator elements could be considered negligible. As a result of the previous work under Contract NAS8-21310 (Reference 1), it is known that the shape of the aperture edge has a pronounced influence on the acoustic resistance of the liner; however, the effect can be predicted if the flow coefficient of the aperture is known. Therefore, cold-flow experiments were conducted to measure the coefficients of the resonator elements before they were installed in the test motor.

Firings with N_2O_4 oxidizer and 50%-N_2H_4-50% UDMH fuel were conducted at nominal test conditions of 100-psia chamber pressure and 1000-lb thrust. Pulse guns were used to trigger combustion instability. From the data the acoustic resistance, reactance, and absorption coefficients of the elements under hot firing conditions, as well as the particle velocities in the element apertures and the incident energy levels, were computed.

C. ACCOMPLISHMENTS

Twenty-five firings of the test motor were conducted; three with a boilerplate chamber and nozzle to check out the test stand control systems, two with the acoustic chamber and the primary injector, and twenty with the acoustic chamber and the backup injector. Of the last

20 firings, no data were obtained from four because of malfunctions, and in 10 of the tests the induced pressure oscillations were suppressed by the acoustic test sections within approximately 20 milliseconds. Steady-state combustion instability was experienced during 6 tests.

Data from which the acoustic parameters were computed consisted of (1) pressure amplitudes at the face of each resonator array element and in the resonator cavities and (2) the phase relation between each pair of pressure signals. Other parameters were the measured gas temperatures in the resonator apertures and cavities and the molecular weight of the cavity gas determined using chromatographic analysis of samples.

A special high sound level generating unit was fabricated for calibration of the phase-measuring system. Calibration involved the measurement of the system-induced phase shift (baseline phase shift) between each two data recording channels used to monitor dynamic pressures at the element facing and in the cavity. Analysis of pre-run and post-run phase calibrations showed that the baseline phase shift was less than 5 degrees; no change in the phase shifts occurred during the test program.

Analysis of the acoustic resistance data computed from the pressure-phase relations showed satisfactory agreement of the hot test data with results obtained from previous cold flow experiments. A comparison of the acoustic reactance data with cold flow data did not show good agreement, but a new correlation was derived from the hot test data. Comparison of the experimental absorption coefficients, also computed from the pressure-phase data, with theory showed an average deviation of 11%.

From the results of these experiments it was concluded that the present theory is satisfactory for use in designing resonator arrays for rocket combustion chambers. It is recommended that the liner design be based on the maximum pressure amplitude at which the combustion in the particular chamber is considered stable.

SECTION II
CONCLUSIONS AND RECOMMENDATIONS

From the results of the work reported herein it is concluded that the present theory as outlined in Reference 1, with the following modifications, be used in designing resonator arrays for rocket combustion chambers:

1. The effective aperture length with no flow through and/or past the apertures be computed from

    $$l_{eff} = T + 0.7D$$

    where T is the facing thickness and D is the aperture diameter (both T and D in inches).

2. The maximum pressure amplitude allowable for combustion in a given motor to be considered stable be used to compute the liner absorption for the motor, instead of the arbitrary 190 db that has been used previously.

Past efforts at Pratt & Whitney Aircraft on absorbing liners have been limited to theoretical analysis and experimental evaluation of designs consisting of arrays of Helmholtz-type resonators. These devices are efficient combustion instability suppressors, primarily because, when properly designed, they can absorb a large percentage, if not all, of the pressure wave energy acting on the surface of the liner. Thus, an array covering a significant portion of the combustion chamber surface is desirable to ensure stable combustion. However, in may instances (particularly cases of existing thrust chambers in which attempts to uprate performance are thwarted by the appearance of combustion instability), surface areas are limited and only a few nonarray acoustic devices such as single resonators, slits, or quarter-waver tubes can be installed. Under this circumstance, the resonator array theory is not valid. In fact, both the absorbing coefficient and the open area ratio, used in the array theory, can only be arbitrarily defined for these devices. Hence, it is recommended that a theory be developed for the design of nonarray acoustic devices for suppression of rocket motor combustion instability.

SECTION III
TEST SERIES

A. HARDWARE DESIGN

The objective of the rocket motor tests conducted was to obtain
impedance and absorption coefficient and particle velocity data for
liner sections during hot firing conditions for comparison with values
predicted using the cold flow based design theory. To avoid effects on
impedance of gas flow past the resonator elements the design of the
test thrust chamber was based on the necessity of having a low Mach
number in the combustion chamber. A contraction ratio of 7.4 was used to
produce a Mach number of 0.08. A chamber diameter of 8.87 inches was
selected to make optimum use of the existing injectors. A chamber
length of 14 inches was required to provide adequate space for the liner
test sections.

Figure III-1 presents the design of the test thrust chamber. There
are six portholes on the chamber wall for mounting any or all of the six
liner test sections. A typical test section is shown in figure III-2,
and the geometry of each section fabricated is given in table I. As
shown in figures III-3 and III-4, each element contains two helium-bleed
pressure transducers (Kistler Model 614A); one to measure pressure oscil-
lations in the liner cavity, and one to measure pressure oscillations at
the liner surface. Two thermocouples are installed to measure the liner
cavity gas temperature and the liner aperture gas temperature. A tube
through the cavity rear wall is used to take hot gas samples for chromato-
graphic analysis. The cavity backing depth of each test section may be
adjusted for a resonant frequency corresponding to any of the first three
transverse modes, the first four longitudinal modes, or the first radial
mode.

FD 33628A
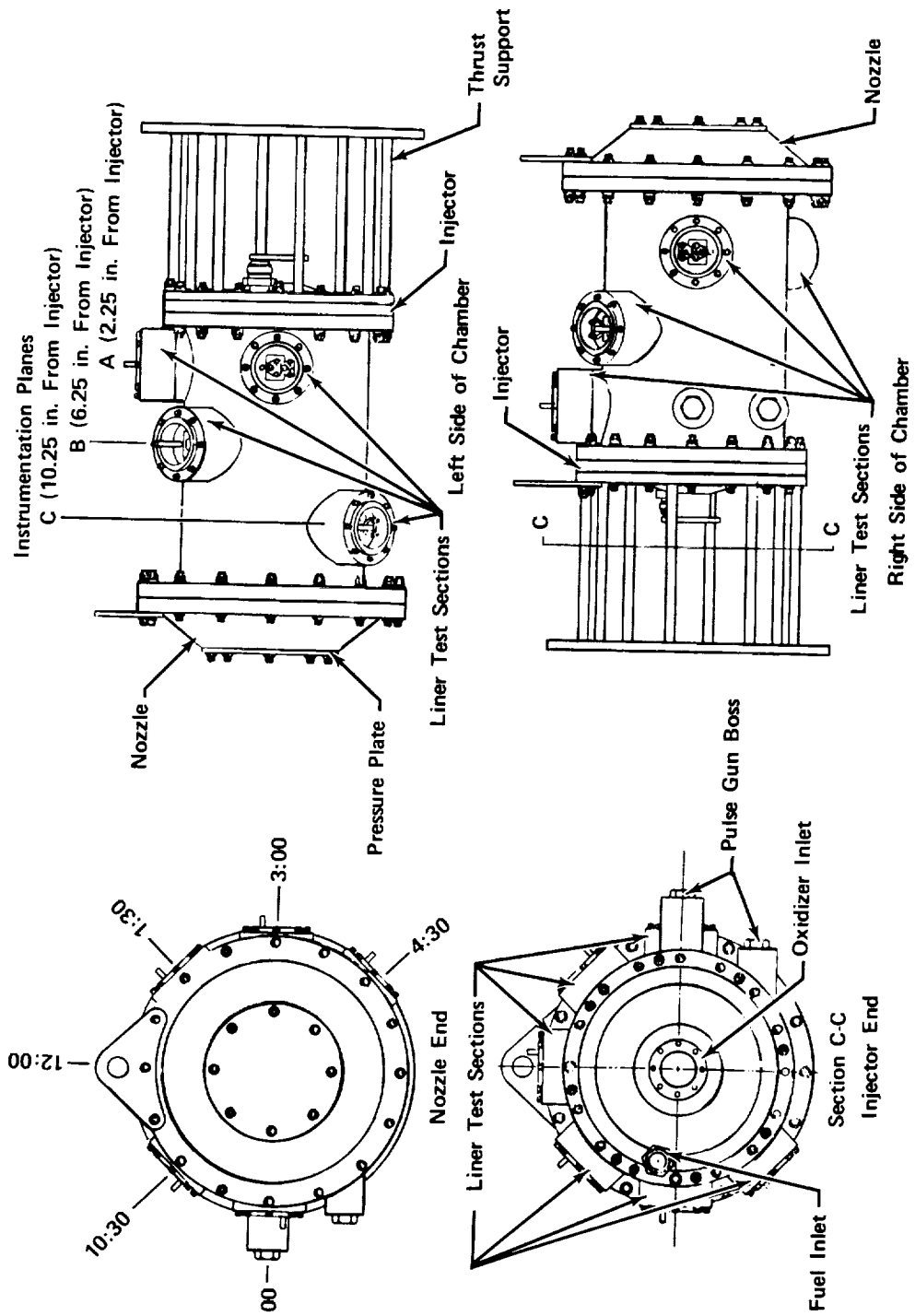
Figure III-1. Test Motor
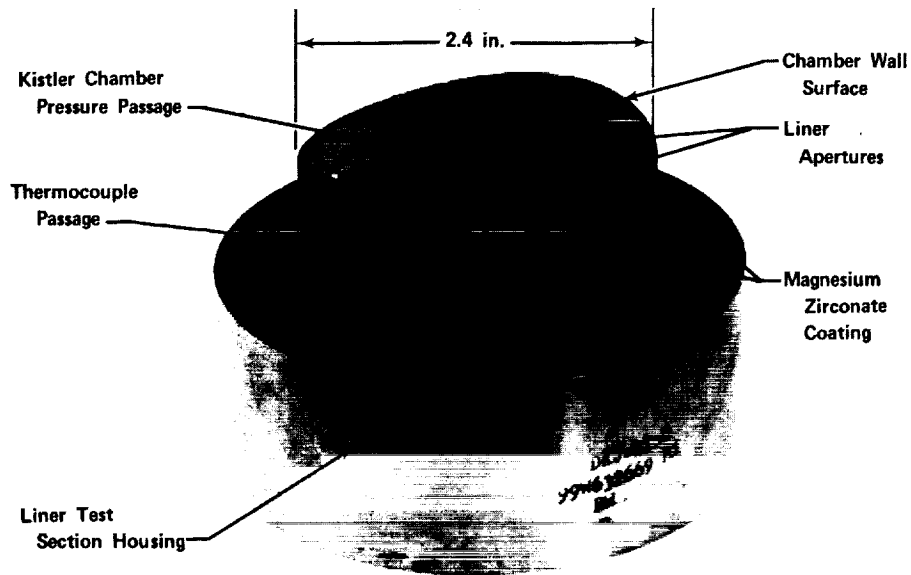
FD 33718A

Figure III-2. Typical Liner Test Section (Facing Side)

Table I.   Resonator Configurations for Test Series

Liner Test Section No.	Liner Thickness (in.)	Open Area Ratio (%)	Range of Cavity Depth (in.)	Aperture Diameter (in.)	Cavity Depth for Maximum Absorption (in.)
1	0.250	2.4	0.15-0.65	0.067	0.150
2	0.200	3.0	0.20-0.70	0.144	0.200
3	0.150	5.4	0.25-0.75	0.111	0.375
4	0.259	5.5	0.15-0.65	0.102	0.275
5	0.200	8.0	0.20-0.70	0.096	0.513
6	0.150	10.8	0.25-0.75	0.094	0.750
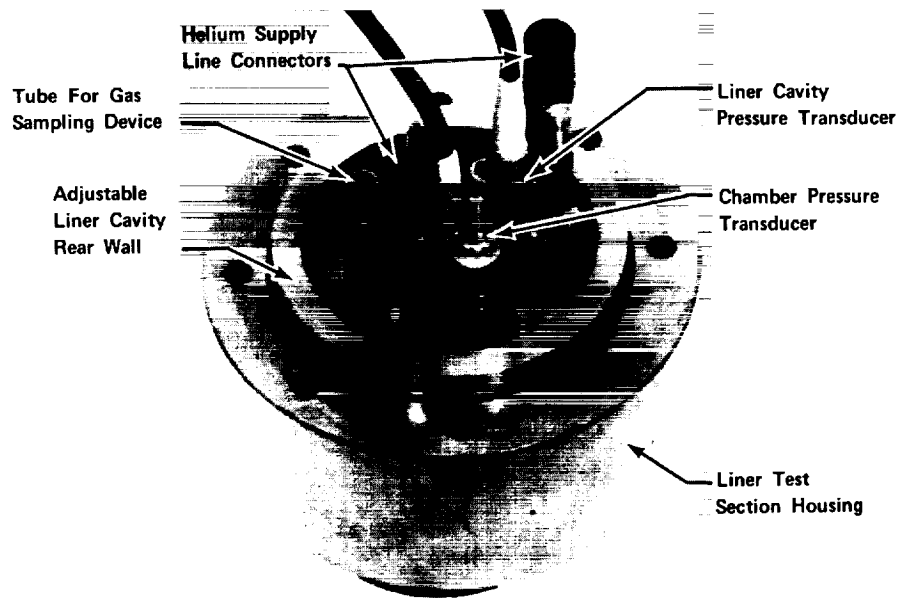
FE 90054   FD 33719

Figure III-3. Rear View of Typical Liner Test Section Show-
ing Instrumentation
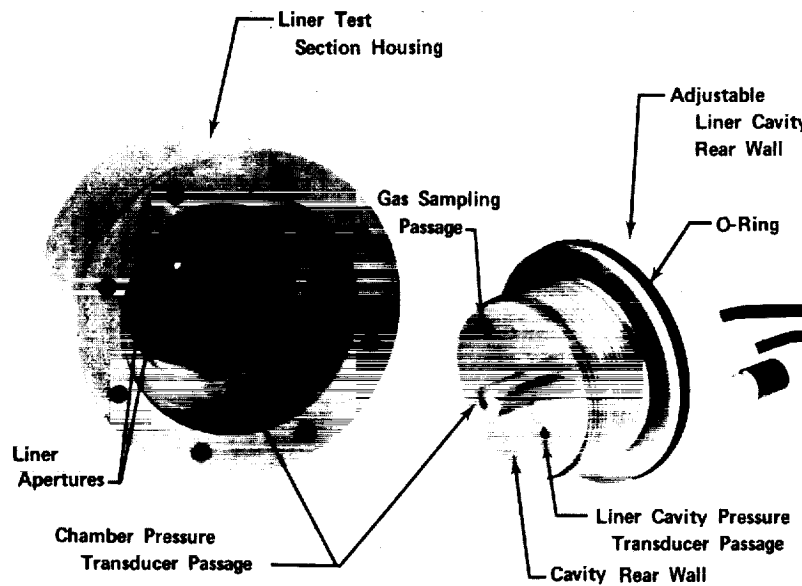
FE 90055

Figure III-4. Liner Test Section (Internal View)   FD 33720

Two existing Pratt & Whitney Aircraft-owned injectors were modified for use under this program. A low-momentum ratio, parallel fan triplet injector (figure III-5) was the primary unit and a self-impinging, radial doublet injector (figure III-6) was the backup injector. To modify the injectors for use in the 1K thrust range, approximately half of the fuel and oxidizer orifices were welded shut. To prevent the formation of dead-end passages where fuel or oxidizer could be trapped, the orifices were plugged with Inconel X rods, etched to the orifice diameter and length, and welded so the entire volume of the passages was filled.

A simple boiler-plate combustion chamber (figure III-7) was designed for preliminary firings. These were planned to check both the primary injector and the test stand control system without risking damage to the instrumented thrust chamber. The boiler-plate chamber was made from 10-inch, Schedule 40, stainless steel pipe. The nozzle was a simple, flatplate orifice.
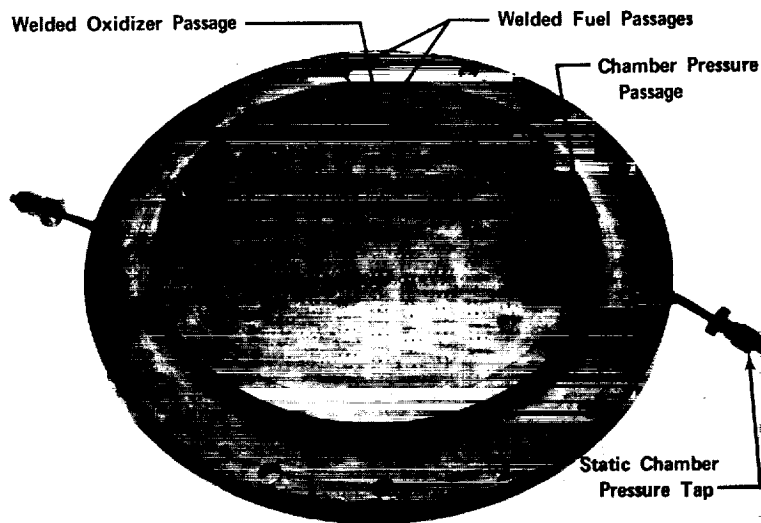
FE 89500
FD 33721

Figure III-5. Modified Low-Momentum Ratio Parallel Fan Triplet Injector

FE 89609
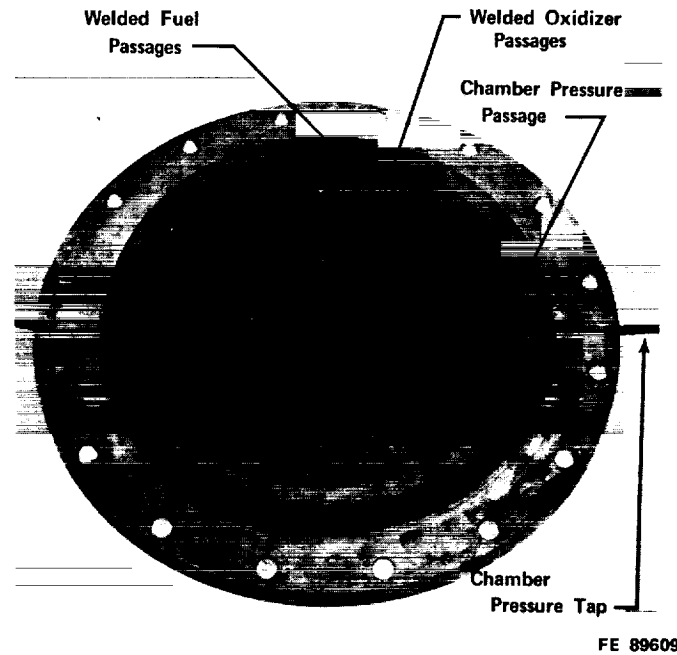
FD 33722

Figure III-6. Modified Self-Impinging Radial Doublet Injector
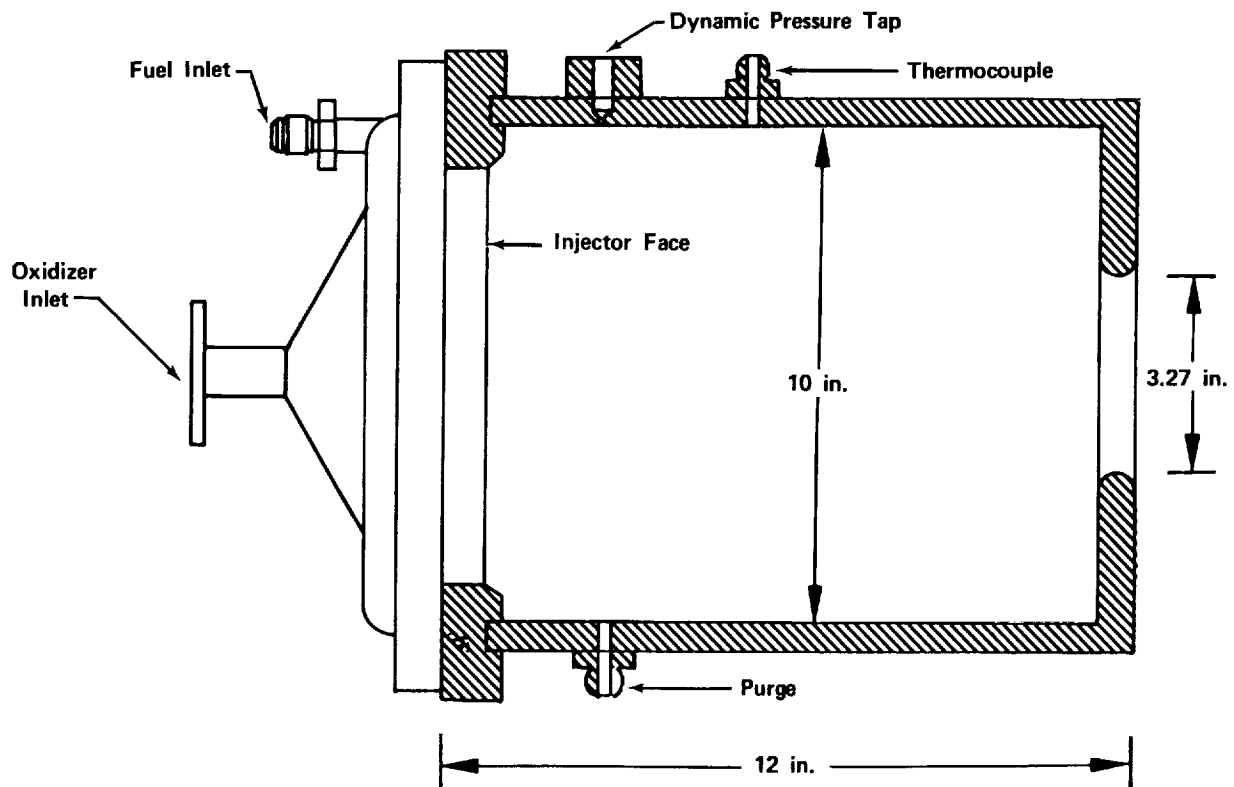
FD 33723A

Figure III-7. Combustion Chamber Used for Preliminary
Checkout Tests

B. CALIBRATION OF PHASE MEASURING SYSTEM

Use of the pressure-phase technique for analyzing acoustical character-
istics of liners in rocket chambers has been attempted previously (Refer-
ence 2), but the results were inconclusive because an exact calibration of
the phase measuring system was not performed prior to testing. Calibration
involves the measurement of the system induced phase shift (baseline phase
shift) between two data recording channels used to monitor the dynamic
pressures in the combustion chamber and in the cavity behind the liner.
If the baseline phase shift is not determined, it is added to the phase
angle being measured, introducing an error of unknown magnitude.

A special high frequency, high sound level generating unit (figure III-8)
was fabricated for calibrating the phase measuring system. The calibration
apparatus consists of four Atlas sound drivers interconnected by a manifold
and exiting into a closed-end tube. Sound pressure levels of 175-db
(Reference 0.0002 microbar) can be generated up to a frequency of
approximately 3000 Hz or 160 db to a frequency of 6000 Hz. The closed
end is formed by a special end-plate (figure III-9) in which two helium-
bleed Kistler pressure transducers (Model No. 614A) and a 1/4-inch
microphone are mounted so that all three can simultaneously monitor the
standing wave pressure oscillations at the end of the tube. The passages
leading from the end of the tube to the Kistler transducers are the same
length and are identical to those used in the liner test sections.

The data acquisition system for transmitting and recording the response
of the Kistler pressure transducers contains twelve channels, two for each
of the six liner test sections. A diagram of two channels is shown in fig-
ure III-10. For each liner test section the dynamic pressures in the
liner cavity and in the combustion chamber at the facing of the liner
test section are recorded. To supply data for determining the baseline phase
shift between two channels, both pressure transducers are mounted in the end
plate of the phase calibrating apparatus. A signal of known frequency is
generated in the tube by the four sound drivers and the amplitude is
monitored with the 1/4-inch microphone. The entrances to both pressure
transducer passages are in the same plane at the end ot the tube; there-
fore, a known phase angle of zero degrees is generated for recording by
both pressure transducer channels.

1/4-in. Condenser Microphone

Kistler Helium Bleed Pressure Transducers

End Plate →

Standing Wave Tube

Helium Supply Line Connectors

Sound Drivers

Sound Drivers
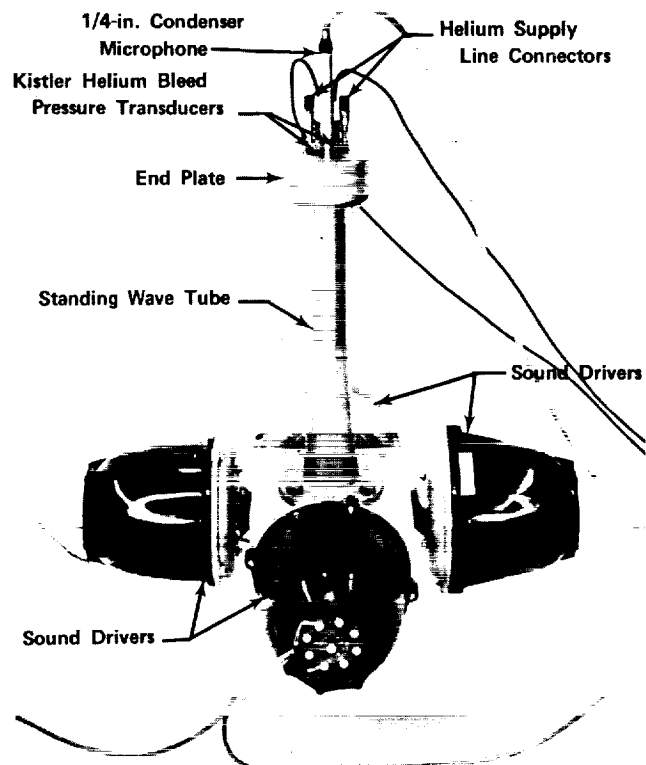
FE 89606

FD 33724

Figure III-8. Phase Shift Calibration Apparatus

Microphone Diaphragm

End Plate

Passages to Pressure Transducers
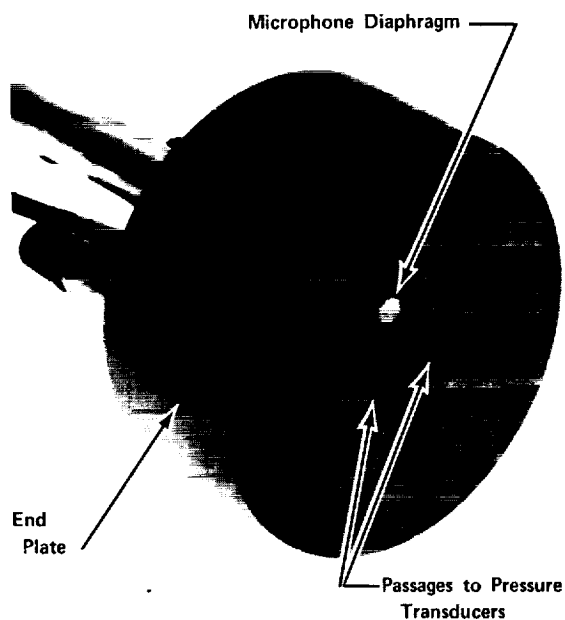
FD 33725

Figure III-9. End Plate for Phase Shift Calibration Apparatus
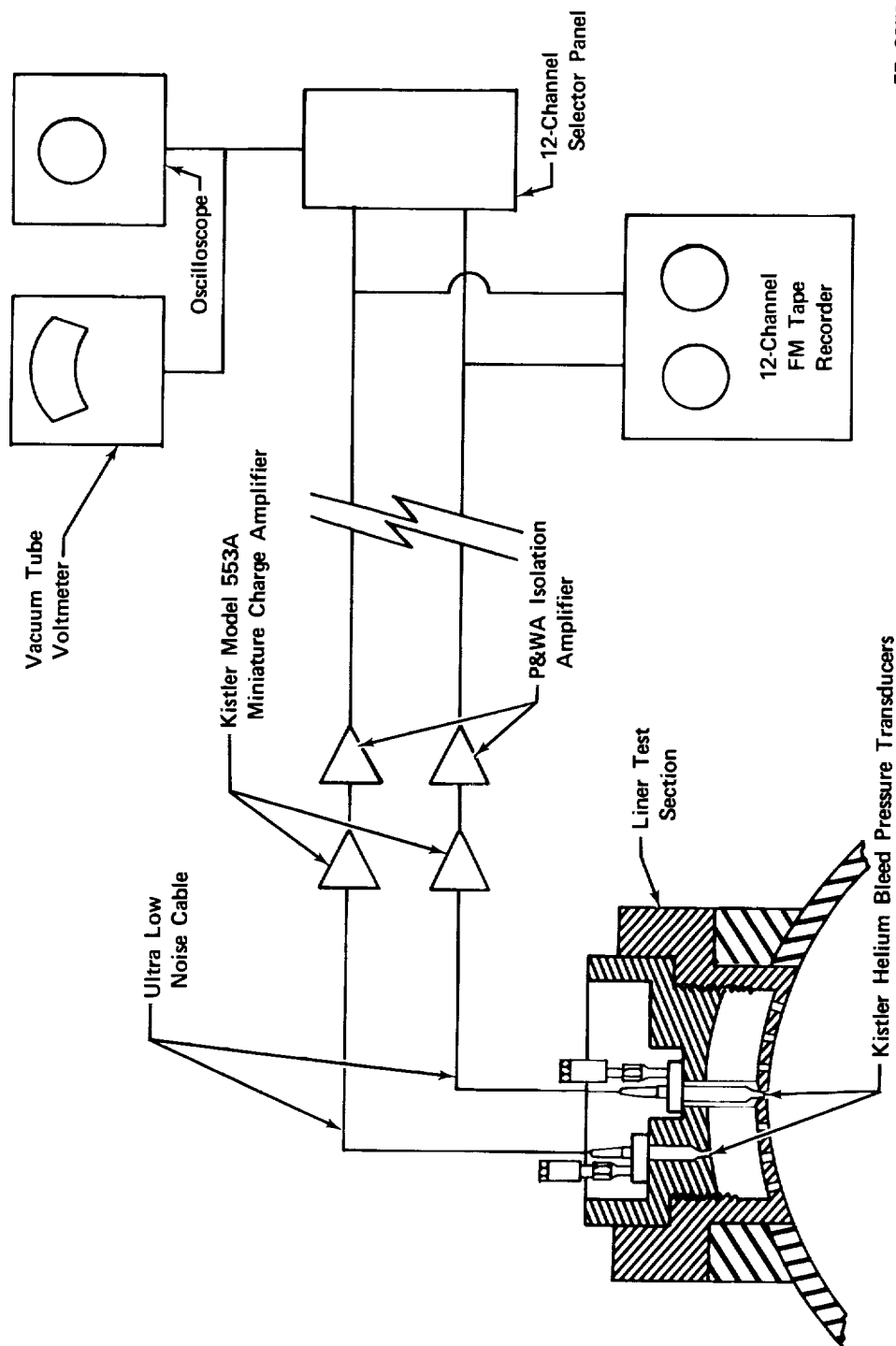
FD 33726

Figure III-10. Typical Data Acquisition System for a Liner Test Section

Calibration tests to provide data for measurement of the baseline phase shift for each of the six sets of dynamic pressure recording channels were conducted before and after the test series. Each set of channels was calibrated over a range of frequencies from 800 to 6500 cps, with dynamic pressure amplitudes up to 3-psi peak-to-peak.

A preliminary determination of the baseline phase shift was made by making a visual measurement of the phase angle between each set of dynamic pressure recording channels. The recorded signals were monitored on a dual beam oscilloscope and phase angles ranging approximately between 0 and 30 degrees were observed. At several frequencies, large distortions in the signals were seen. These were caused by harmonic frequencies present in the calibration apparatus and indicated that filtering of the recorded signals would be necessary to eliminate the distortion and permit determination of baseline phase shift at the fundamental frequency.

C. TEST PROGRAM

Twenty-five hot firings were made on the FRDC B-5 test stand. A summary of the tests is presented in table II. Three initial tests were made with a boilerplate chamber to ensure proper operation of the modified triplet injector and to check out the test stand control system. During the first firing (test No. 1.01), the oxidizer flowmeter that is used as a controls sensor, malfunctioned, resulting in a maximum oxidizer flow with a corresponding 35% overscale in chamber pressure. Run time was two seconds; no hardware damage resulted. During test No. 2.01, the control system operated properly; however, it was found that 1.8 seconds were required to reach steady-state chamber pressure. The slow response of the motor was caused by the low flowrates required for a thrust of 1000 pounds; 1.6 seconds were required to fill the supply lines and injector manifolds with propellants. The firing duration for test No. 3.01 was increased to 3.0 seconds; no heat transfer problems were encountered, and a dynamic pressure transducer (Kistler Model 614A) indicated that no combustion instability was present. All control systems were functioning properly, and no problems were encountered with the modified injector; therefore, the boilerplate chamber was replaced with the acoustic element chamber.

Table II. Test Summary

Test No.	Liners Used	Pulser Charge	Cavity Depth in.	Abort	Comments
1.01	None	None		No	Boilerplate chamber, oxidizer control valve malfunction; chamber pressure was 135 psia
2.01	None	None		No	Boilerplate chamber; run was too short to get steady chamber pressure
3.01	None	None		No	Run duration was 3.0 seconds; No controls or injector problems
4.01	None	None		No	Used acoustic chamber with solid plugs; no instability
5.01	None	16-Grain Tangential			16-Grain pulser at +2.3 seconds caused 100 psi peak-to-peak amplitudes that damped in 30 milliseconds
		20-Grain Radial		No	20-Grain pulser at +2.7 seconds caused 150 psi peak-to-peak amplitudes that damped in 80 milliseconds
6.01	None	16-Grain Tangential			Using radial doublet injector, 16-grain pulser initiated peak-to-peak amplitudes of about 80 psi
		20-Grain Radial		RCC	Abort at +2.4 seconds
7.01	All	6-Grain Tangential	Minimum Depth (See table II.)	No	Oxidizer injector passages clogged; chamber pressure at about 50 psia
8.01	All	10-Grain Tangential	Minimum Depth	High TC	Same as 7.01; abort caused by temperature spike that occurred when pulse gun was fired
9.01	All	16-Grain Tangential	Minimum Depth	No	Pressure perturbation damped in 20 milliseconds

Table II. Test Summary (Continued)

Test No.	Liners Used	Pulser Charge	Cavity Depth in.	Abort	Comments
10.01	All	16-Grain Tangential 20-Grain Radial	Minimum Depth	No	Pressure perturbation damped in 20 milliseconds
11.01	3.0% (3:00A) 8.0% (12:00A)	25-Grain Tangential	0.3250 0.3250	RCC	100 milliseconds of 60- to 80-psi peak-to-peak data
12.01	3.0% (3:00A) 5.5% (10:30B) 8.0% (12:00A)	25-Grain Tangential	0.5125 0.2750 0.5125	High TC	Test aborted immediately after pressure pulse
13.01	3.0% (3:00A) 5.5% (10:30B) 8.0% (12:00A)	40-Grain Tangential	0.5125 0.2750 0.5125	No	Pressure disturbance damped in 20 milliseconds
14.01	3.0% (3:00A) 8.0% (12:00A)	6-Grain Tangential	0.5125 0.5125	No	Pulser disturbance damped in 20 milliseconds
15.01	3.0% (3:00A) 8.0% (12:00A)	25-Grain Tangential	0.6375 0.6375	RCC	100 milliseconds of 50- to 80-psi peak-to-peak data
16.01	2.4% (3:00A) 10.8% (12:00A)	25-Grain Tangential	0.150 0.375	RCC	100 milliseconds of 30- to 40-psi peak-to-peak data
17.01	2.4% (3:00A) 10.8% (12:00A)	25-Grain Tangential	0.375 0.5625	No	10 milliseconds of 30-psi peak-to-peak data
18.01	2.4% (3:00A) 10.8% (12:00A)	25-Grain Tangential	0.525 0.750	No	Pressure pulse damped in 10 milliseconds
19.01	10.8% (12:00A)	25-Grain Tangential	0.750	No	Pulser spike damped in 15 milliseconds
20.01	5.4% (3:00A) 5.5% (12:00A)	25-Grain Tangential	0.250 0.150	RCC	100 milliseconds of 40- to 60-psi peak-to-peak data
21.01	5.4% (3:00A) 5.5% (12:00A)	25-Grain Tangential	0.375 0.275	No	10 milliseconds of 20-psi peak-to-peak data

Table II. Test Summary (Continued)

Test No.	Liners Used	Pulser Charge	Cavity Depth in.	Abort	Comments
22.01	5.4% (3:00A) 5.5% (12:00A)	25-Grain Tangential	0.625 0.525	No	No acceptable data obtained because of a chugging instability
23.01	5.4% (1:30B) 5.5% (10:30B)	25-Grain Tangential	0.375 0.275	RCC	100 milliseconds of 60-psi peak-to-peak data
24.01	8.0% (1:30B) 10.8% (10:30B)	25-Grain Tangential	0.5125 0.7500	No	Approximately 100-psi spike damped in 20 milliseconds
25.01	2.4% (1:30B) 10.8% (10:30B)	25-Grain Tangential	0.150 0.7500	No	Approximately 100-psi spike damped in 20 milliseconds

Tests No. 4.01, 5.01, and 6.01 were made using the acoustic element chamber with the liner test section portholes closed using solid plugs to enable the dynamic pressure characteristics of the unlined chamber to be obtained. Test No. 4.01 was a stable run in which no perturbation devices were used. For test No. 5.01, a 16-grain tangential pulser, timed to fire at +2.3 seconds and a 20-grain radial pulser timed to fire at +2.7 seconds, were installed. The run was stable until the tangential pulser fired, causing an overpressure in excess of 100 psi that damped in 25 milliseconds; firing the radial pulser resulted in an overpressure in excess of 150 psi that damped in 80 milliseconds. In an attempt to obtain a more unstable motor, the injector was replaced before test No. 6.01 with the radial doublet fan injector. A 16-grain tangential pulser and a 25-grain radial pulser were installed and timed to fire as in test No. 5.01. The run was stable until the tangential pulser fired, causing an overpressure in excess of 100 psi that failed to damp. The pressure oscillations were primarily at a frequency corresponding to the first tangential mode (2980 cps) with peak-to-peak amplitudes up to 100 psi. (See figures III-11 and III-12.) The test was aborted at +2.4 seconds by the Rough Combustion Cutoff device (RCC). No hardware damage was encountered.

From the results of test No. 6.01, it was concluded that the motor with the radial doublet injector was dynamically unstable and, therefore, suitable for testing with the acoustic elements. The solid plates were removed and the six acoustic liner test sections were installed.

Four tests (No. 7.01, 8.01, 9.01, and 10.01) were made with all six liners installed (figures III-13 and III-14) and set at their minimum cavity depth. (Refer to table I.) In tests No. 7.01 and 8.01, insufficient data were obtained because of a 50% underscale in chamber pressure. The low chamber pressure was the result of low oxidizer flow caused by clogging of the oxidizer injector passages with the residue of a reaction between the nitrogen tetroxide and moisture in the atmosphere. The passages were cleaned by flowing demineralized water through the injector; to prevent recurrence, a heated gaseous nitrogen purge was used between firings throughout the remainder of the test program.
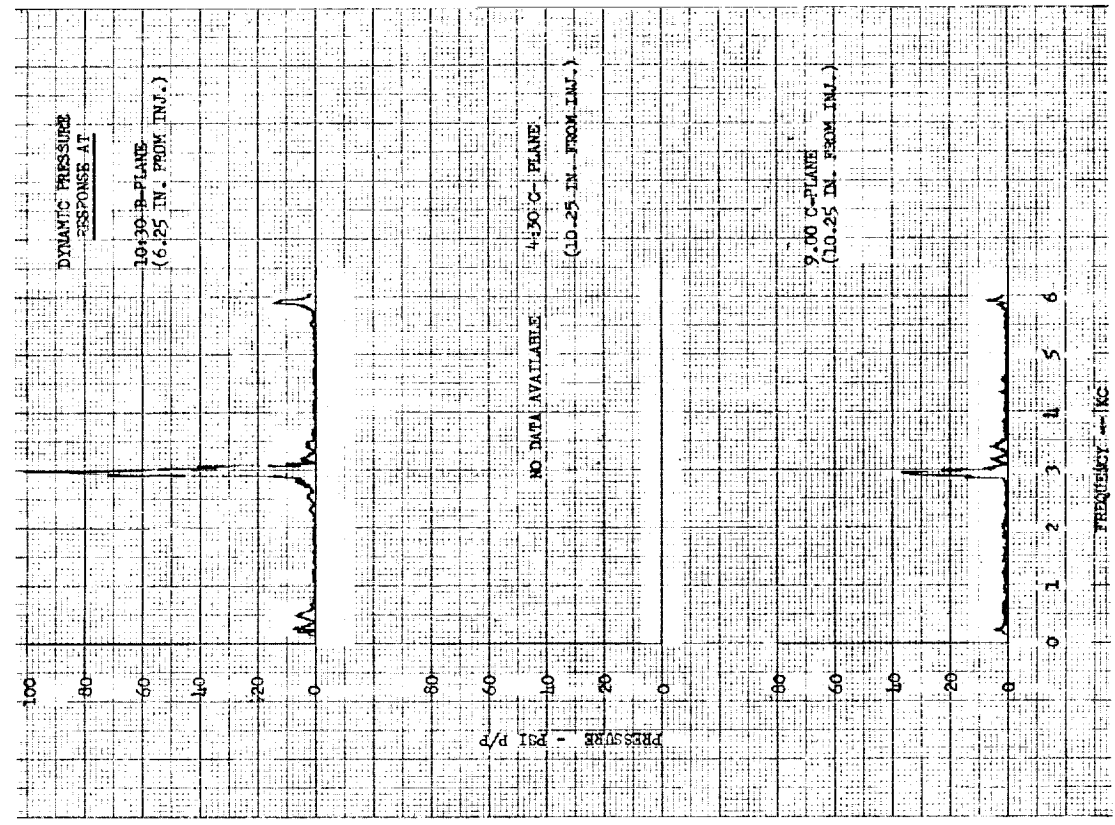
DF 77986

Figure III-12. Dynamic Pressure Charac-
teristics of Chamber -
Test No. 6.01
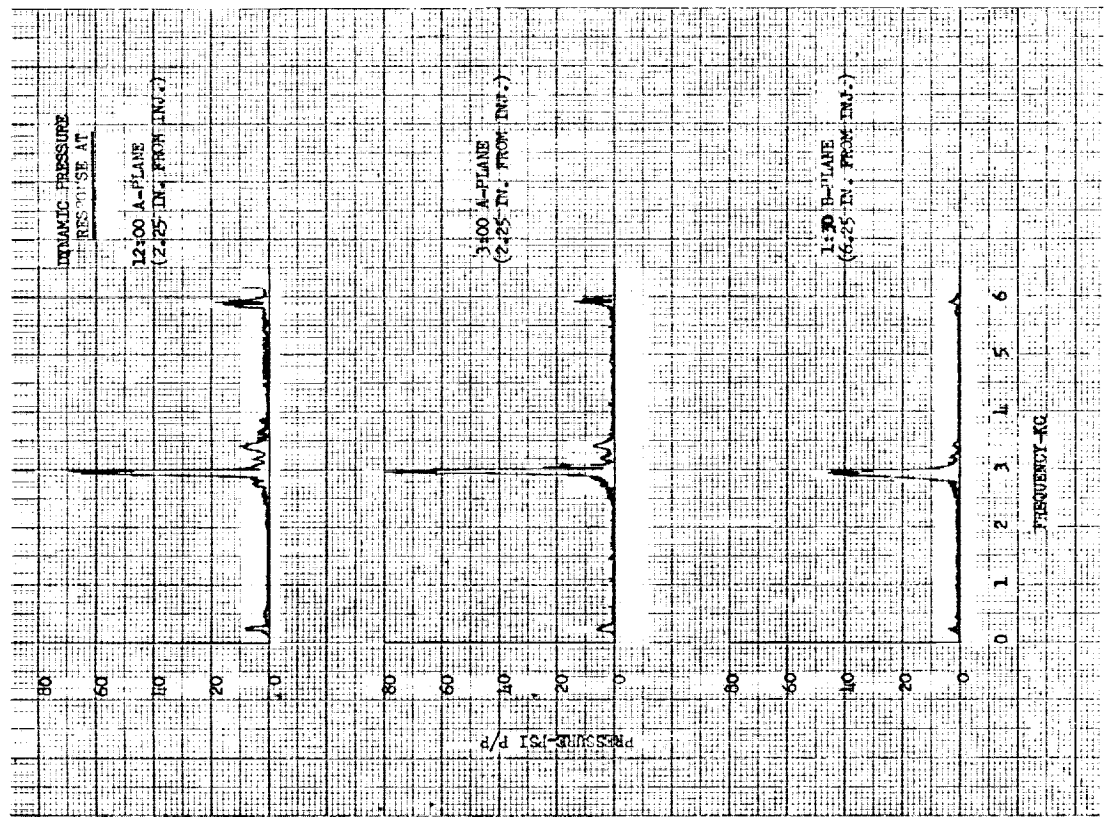
DF 77985

Figure III-11. Dynamic Pressure Charac-
teristics of Chamber -
Test No. 6.01
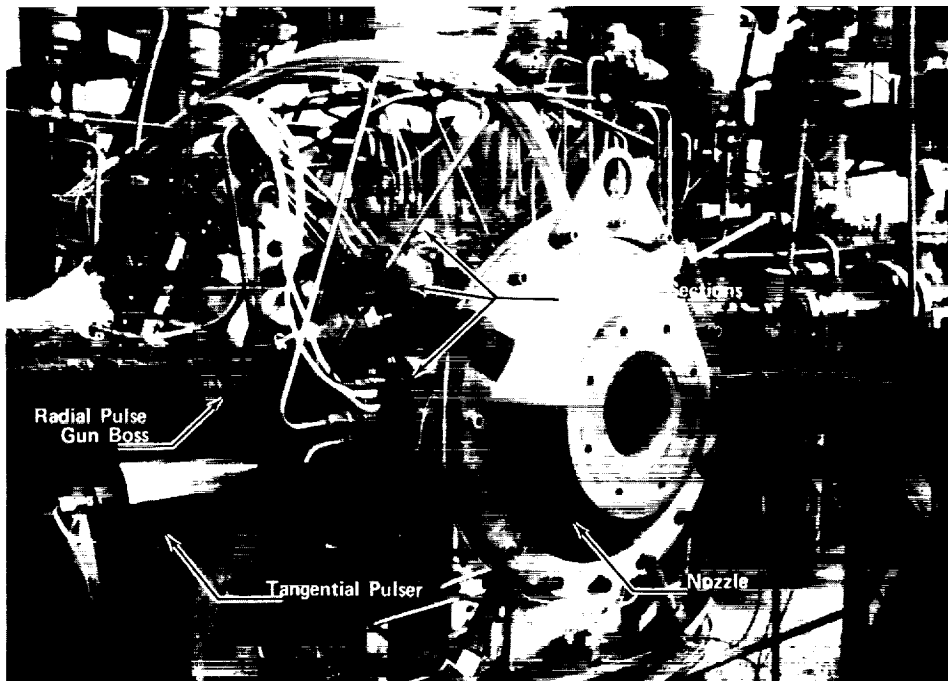
FD 36173

Figure III-13. Combustion Chamber With Acoustic Test
Sections Installed
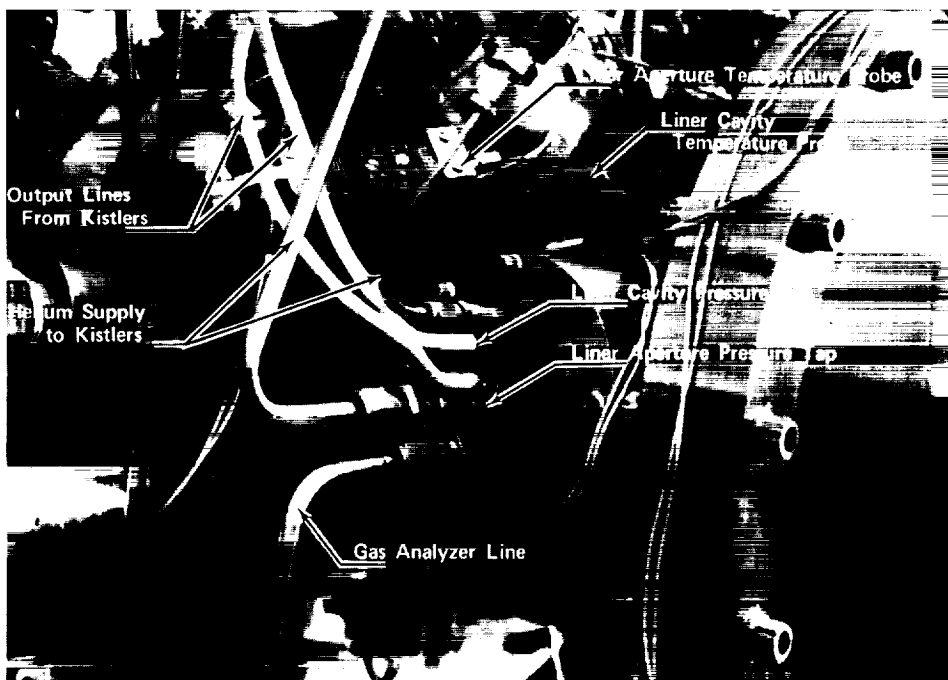
FD 36175

Figure III-14. Typical Liner Test Section

In test No. 9.01, a 16-grain tangential pulser was fired at +2.3 seconds, producing an overpressure in excess of 100 psi that damped in 20 milliseconds. For test No. 10.01, a 16-grain tangential pulser and a 20-grain radial pulser were both timed to fire +2.3 seconds. An overpressure in excess of 250 psi resulted, which again damped in about 20 milliseconds.

From the results of test No. 10.01, it was concluded that the motor could not be driven unstable with all six acoustic elements installed; therefore, four liner test sections were removed from the B and C planes leaving only the 3.0% and the 8.0% liner samples nearest the injector in the A-plane. (See figure III-1 for location and angular orientation of instrumentation planes.) Both liner cavity depths were set for low absorption at the first tangential mode.

During test No. 11.01, combustion was stable until the 25-grain tangential pulser was fired at +2.3 seconds, causing an overpressure in excess of 200 psi and producing pressure oscillations of approximately 80-psi peak-to-peak that failed to damp. The test was aborted at +2.4 seconds by the RCC system.

In an attempt to reduce the number of firings required to test all of the liner samples, a third liner test section was added in the 10:30 B-plane position before test 12.01. The liner cavity volume was adjusted for maximum absorption at the first tangential mode. Test No. 12.01 was aborted because of a malfunction in the high temperature abort system; no acoustic data were obtained. Test No. 13.01 was made immediately after run 12.01, with no changes to the liners. A 40-grain tangential pulser was fired at +2.3 seconds, but the resulting pressure disturbance was damped in 20 milliseconds. Evidently, the addition of the third liner sample provided too much absorption; therefore, the liner sample in the B-plane was removed before the next run. During test No. 14.01 the pressure perturbation was damped in 20 milliseconds. For test No. 15.01, the backing cavity depth of the two liners was increased to reduce the amount of absorption at the first tangential mode. A 25-grain tangential pulser was fired at +2.3 seconds resulting in approximately 80-psi peak-to-peak pressure oscillations that did not damp; an RCC abort occurred at +2.4 seconds.

The next four tests were made with the 10.8% open area ratio liner in the 12:00 A-plane position and the 2.4% liner in the 3:00 A-plane position. For test No. 16.01, the 2.4% liner was set for maximum absorption and the 10.8% liner was set for minimum absorption. Beginning with Test No. 16.01, a gas analyzer was connected so that the gas density in the liner cavities could be determined. A 25-grain tangential pulser was fired, causing pressure oscillations of about 40-psi peak-to-peak that failed to damp; an RCC abort occurred. For tests No. 17.01 and 18.01, the backing cavity depth was increased before each run, and a 25-grain tangential pulser was fired during each test; the pressure pulses damped in less than 20 milliseconds. Before the next test, the 2.4% liner was removed leaving only the 10.8% liner set for maximum absorption at the first tangential mode. A 25-grain tangential pulser fired at +2.5 seconds created a 200-psi pressure spike that was damped in 10 milliseconds. It was concluded that the 10.8% liner absorbed sufficient energy to provide stable combustion regardless of the amplitude of the perturbations.

In the next three tests, the 5.5% liner sample was installed in the 12:00 A-plane position, and the 5.4% liner was installed in the 3:00 A-plane position. For test No. 20.01, the liner sections were set at the minimum cavity depth to produce low absorption. A 25-grain tangential pulser was fired at +2.5 seconds, causing approximately 50-psi peak-to-peak pressure oscillations; an RCC abort occurred at +2.6 seconds. For test No. 21.01, both liner cavities were adjusted for maximum absorption at the first tangential mode. A 25-grain tangential pulser was fired causing a pressure spike of over 200 psi that damped in 10 milliseconds. The liner cavity volume was then increased for the next test. Prior to test No. 22.01, the sensitivity of the fuel control valve was changed in an attempt to stop a slight drifting of the static chamber pressure present during earlier firings. Test No. 22.01 was made, but further problems with the fuel control valve sensitivity resulted in a low frequency, high amplitude chugging instability; no acoustic data were obtained. Before test No. 23.01, the fuel control valve sensitivity problem was corrected.

To obtain data from the liner test sections in their resonant configurations, three final tests were conducted with the sections mounted

in the B-plane positions. It was expected that by moving the resonators farther away from the injector it would be easier to excite an instability. Test No. 23.01 was made with the 5.4% liner in the 1:30 B-plane position and the 5.5% liner at the 10:30 B-plane position, both set for maximum absorption at the first tangential mode. A 25-grain tangential pulser was fired at +2.5 seconds that caused 60-psi peak-to-peak oscillations, which persisted until an RCC abort occurred at +2.6 seconds. Also, during test No. 23.01, a gas analyzer was attached to the resonator in the 1:30 B-plane position to sample the cavity gas during the test. Prior to test No. 24.01, the 5.4% and 5.5% liners were removed and the 8.0% and 10.8% liners installed at the 1:30 B-plane position and the 10:30 B-plane position, respectively. The gas analyzer was connected to the 10:30 B-plane position. A 25-grain tangential pulser, fired at +2.5 seconds, produced a 100-psi overpressure, but was damped in 20 milliseconds. In an attempt to reduce the amount of absorption provided by the two acoustic elements, the 8.0% liner was replaced with the 2.4% liner, set to operate at resonance. Test No. 25.01 was made with a 25-grain tangential pulser that produced a 100-psi pressure spike that damped in 20 milliseconds. The last two tests, with the 10.8% liner set at resonance, show that this one liner provides enough absorption to cause this particular combustion chamber to be dynamically stable.

With test No. 25.01, the test program was completed. The results of the 25 tests showed that for this particular thrust chamber instabilities could only be sustained using liners with theoretical absorption coefficients of less than 55%, while liners set for higher absorption caused the pressure oscillations resulting from nonlinear perturbations to decay within 20 to 30 milliseconds.

D. ANALYSIS OF DATA

A discussion of the procedures that were used in reduction and analysis of data from the test series and the results obtained is presented in the following order:

1. Test Stand Oscillograph Traces
2. Aperture and Cavity Gas Temperatures
3. Liner Cavity Gas Analysis
4. Pressure-Phase Data Reduction
5. Analysis of Acoustic Data.

1. Test Stand Oscillograph Traces

Unfiltered oscillograph traces of the response from dynamic pressure transducers are available immediately after each firing is completed. The traces are used to determine the dynamic pressure characteristics of the combustion process after the pulse gun is detonated. The traces indicate how fast the pressure spike decays or, if a steady-state instability is generated, they provide approximate information on the amplitude and frequency of the instability. For example, in test No. 14.01, the 8.0% and 3.0% open area ratio liners (table II) were installed in the chamber; oscillograph traces for the 8.0% liner (figure III-15) indicated that a pressure spike in excess of 100 psi damped in less than 40 milliseconds. In test No. 15.01, the same liners were used but the backing cavity depth was increased by 0.125 inch; oscillograph traces for the same liner indicated that the pressure spike failed to damp, resulting in steady-state pressure oscillations with amplitudes ranging from 50- to 80-psi peak-to-peak. Traces for test No. 15.01 showed the frequency of instability to be approximately 3000 cps (first tangential mode). Unfortunately, these oscillograph traces are not accurate enough to provide exact values for pressure amplitude and frequency; therefore, a more detailed analysis of the tape-recorded signals was performed (see Appendix A).

2. Aperture and Cavity Gas Temperatures

Data from thermocouples installed in the liner apertures and backing cavity are used to provide the information necessary to calculate the density and sonic velocity of gases in the liner. Also, the temperatures recorded from the liner cavity can be useful in determining if combustion gases enter the cavity, or if the helium purges from the pressure transducers maintain a helium atmosphere in the cavity. For example, test No. 11.01 was aborted by the rough combustion cutoff system at approximately +2.46 seconds, or about 0.16 second after the pulse gun detonated. Immediately after the pressure spike occurred, a sharp rise in the aperture gas temperature resulted (figure III-16), with a similar but less abrupt rise in cavity gas temperature. In test No. 13.01, the pressure pulse damped in 20 milliseconds, resulting in stable combustion; the

temperature data indicated only a small change in the rate of temperature
increase. (See figure III-17.) Analysis of the temperature data for
these two tests leads to the conclusion that the high gas temperatures
are the result of unstable combustion and indicates that the gases in
the liner cavity will have the same properties as those of the combustion
gases and not those of helium.
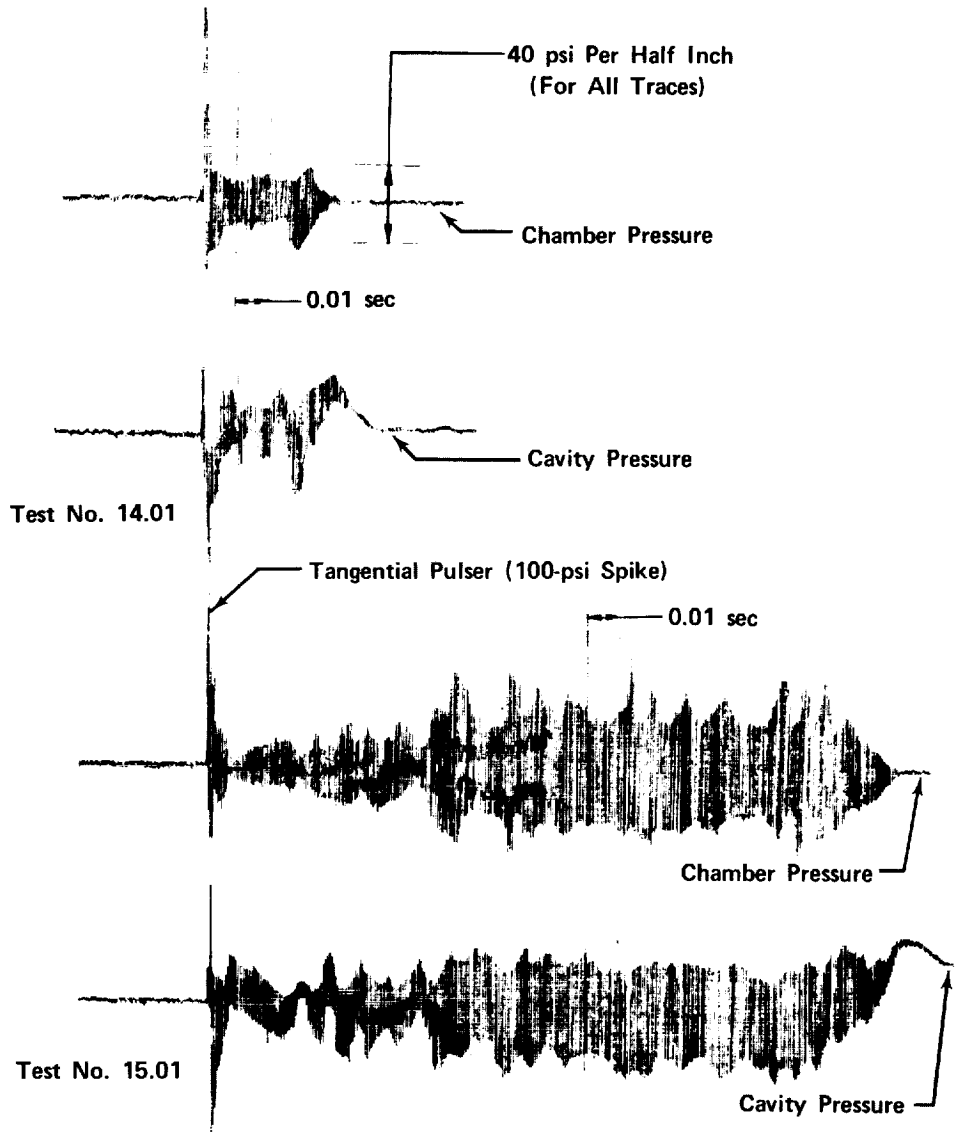
FD 36174

Figure III-15. Oscillograph Traces of 8.0% Liner Tests
No. 14.01 and 15.01
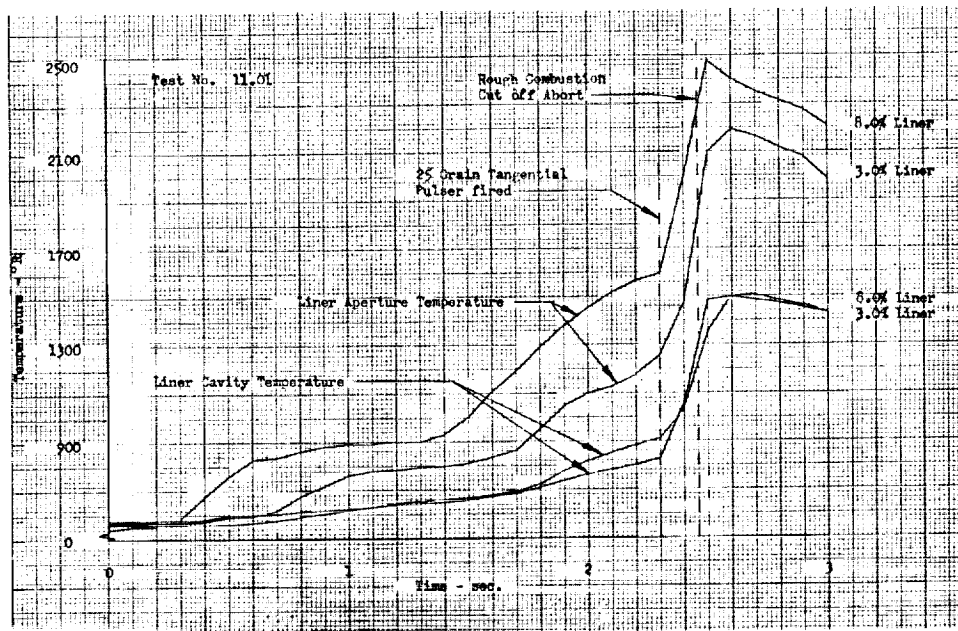
DF 77987

Figure III-16. Liner Aperture and Cavity Temperature Profiles
for Test No. 11.01
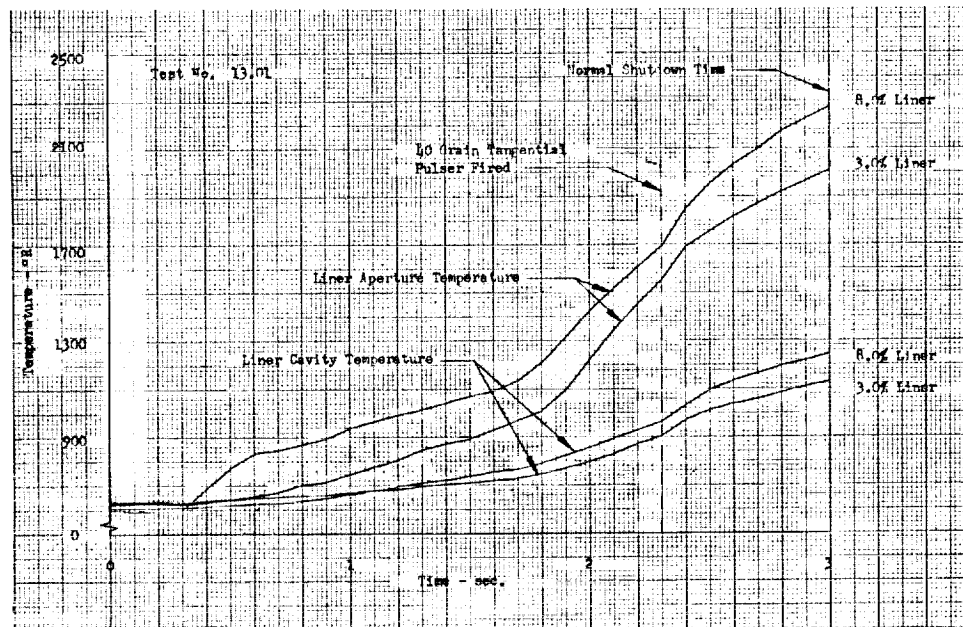
DF 77989

Figure III-17. Liner Aperture and Cavity Temperature Profiles
for Test No. 13.01

3. Cavity Gas Analysis

A gas analyzer was used to determine the average molecular weight of the gases in the liner cavities during several of the hot tests. A measure of the molecular weight was necessary to definitely determine if helium from the pressure transducers, hot gases from the combustion chamber, or a mixture of both were present in the liner cavity. The procedure for determining the molecular weight is as follows.

As shown in figure III-18, the gas sample, forced by the chamber pressure, exits from the liner cavity into the 1st-Varian Aerograph, 6-way linear gas sampling valve. Actuator No. 1 closes at the desired sampling time (0.10 second after the pulse gun fires), and gas is allowed to drop to ambient pressure before actuator No. 2 closes (1.5 seconds after actuator No. 1 closes). The precise sample volume (1 cc) is injected into the nitrogen sample carrier flow to a Gow-Mac Gas Density Detector, Model 373.

The Gow-Mac Density Detector detects changes in flow through the use of heated wire elements in a bridge circuit (E_1 and E_2). A reference gas (gaseous nitrogen) enters the detector (at A), splits into two streams, flows past the detector elements and exits to the atmosphere (at C). The sample enters the detector downstream of the heated elements (at B), splits into two streams, combines with the reference gas flow, and is discharged to the atmosphere.

When the sample gas is the same density as the reference gas, the detector bridge circuit is balanced. When a sample of different density is injected into the detector, the sample density causes a net upward, or downward flow in the detector. The flow variation causes an imbalance in the bridge circuit that is recorded on the Sargent Laboratory Recorder. The difference between the molecular weight of the sample gas and the reference gas is linear with the bridge output for equal gas volumes. The molecular weight of the gas can thus be determined.
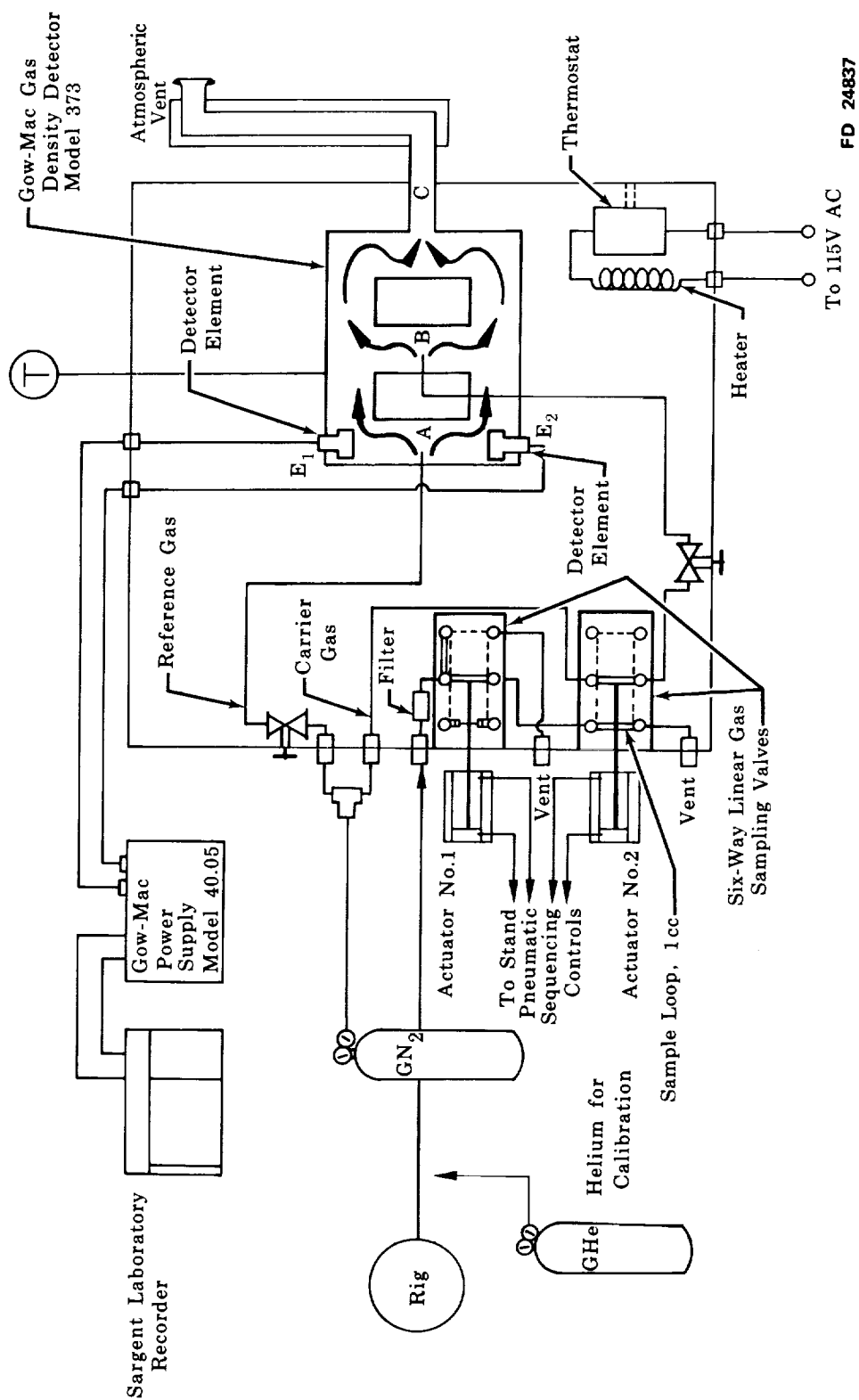
FD 24837

Figure III-18. Schematic of Gas Sampling Molecular Weight Measurement

Results from the gas analyzer data for tests No. 17.01, and 19.01 showed that the gases in the liner cavities were of molecular weight (58 lb_f-ft/lb_m-°R) lower than the theoretical value for combustion gases (70 lb_f-ft/lb_m-°R). It is worthy of note that both tests stabilized immediately after the pulse gun fired. Gas analyzer data from test No. No. 23.01, which was aborted by the RCC, showed that the molecular weight of the gas in the liner cavity was 67 lb_f-ft/lb_m-°R, which is excellent agreement with the theoretical value. From these results, it was con- cluded that for unstable tests the liner cavities are thoroughly purged by hot combustion gases forced into the cavity through the liner aper- tures by the high oscillatory pressure amplitudes in the chamber.

4. Pressure-Phase Data Reduction

Pressure-phase data was obtained from high speed oscillograph traces of the Kistler transducer signals. Before the oscillograph traces were made, a spectral analysis of the dynamic pressure data was conducted. The analysis showed that pressure oscillations above the random noise level, i.e., approximately 1-psi peak-to-peak, existed at three distinct fre- quencies. The amplitudes of two of the oscillations were below 5-psi peak-to-peak; one at a low frequency, which was attributed to 60-cycle noise, and the other at a frequency of approximately 6K Hz, which cor- responded to the first radial mode. The third oscillation was of high amplitude (nominally 50 psi peak-to-peak) at a frequency of approximately 2800 Hz. (The results of the spectrum analysis for these oscillations are included in Appendix A.) Thus, to eliminate all but the high amplitude signals the data was filtered using a 1.6K Hz high pass filter and a 4K Hz low pass filter leaving a frequency band of ±1.2K Hz about the frequency of the first tangential mode.

The high speed oscillograph traces were made by running the oscillograph paper at approximately 160 inches per second (ips) while the data originally recorded on magnetic tape at 30 ips was played back at 1.875 ips. By playing the data back at this reduced speed a higher resolution (spreading out) of the data is obtained, enabling a more precise measurement of the phase angle than if the data were played back at 30 ips. All channels in the oscillograph were ac-coupled to eliminate the dc drift that is caused

by variations in chamber pressure (primarily a result of the shock wave produced when the pulse gun was fired).

The phase angle and pressure amplitudes were taken from the oscillograph traces by hand measurements. The phase angle between two traces was determined by locating the zero point of each pressure wave (figure III-19), and by measuring the distance between them. The phase angle was calculated from the following relationship:

$$\frac{\text{Phase Angle}}{\text{Distance Between Zero Points}} = \frac{360 \text{ degrees}}{\text{Wave Length Distance}} \quad (1)$$

The vertical scale of the traces was set so that a distance of 1 inch represented 60 psi peak-to-peak; hence, the amplitude was calculated from the equation:

$$\text{Pressure Amplitude} = \text{peak-to-peak displacement, in.} \times 60 \quad (2)$$

Oscillograph traces (figure III-20) of the baseline phase calibrations at a frequency of 2800 Hz showed that the system induced phase shift was less than 5 degrees, which is within the accuracy limits of the method used for measurement. Furthermore, comparison of prerun and postrun calibration data (figure III-20) indicated that the baseline phase shift was the same before and after the test program. Therefore, the baseline phase shift used for correcting the phase angles obtained from the hot test data was taken as zero.

5. Analysis of Acoustic Data

To determine the acoustic characteristics of each liner test section, the impedance relations derived in Reference 1 were used to determine the components of impedance, orifice particle velocity, absorption coefficient, and incident sound pressure levels from each data point (including the pressures in front of the liner, in the liner cavity, and the phase angle between the two). All data, including the computed acoustical characteristics, are listed in Appendix A.

Portion of Oscillograph Trace for Hot Fire Test No. 15.01
$\sigma = 8.0\%$ L = 0.6385 in.
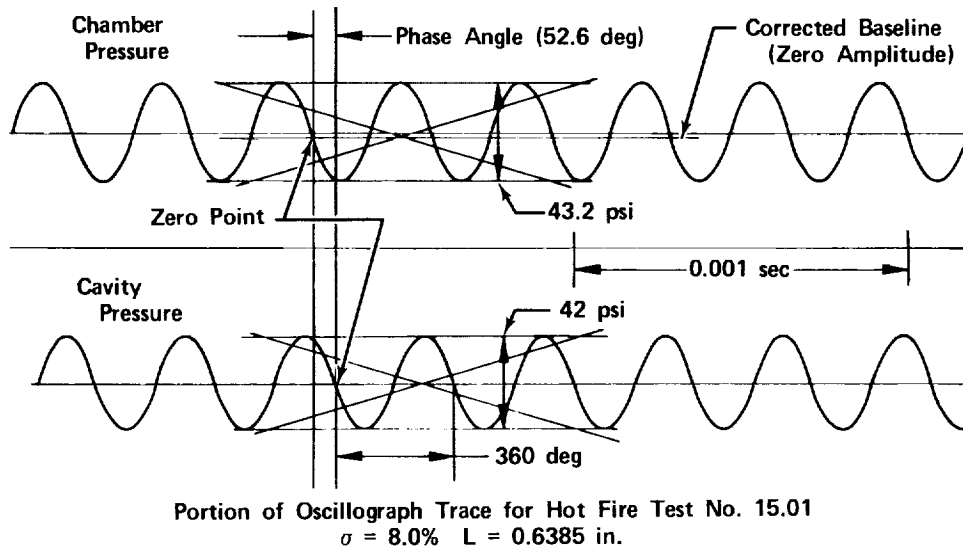
FD 37874

Figure III-19. Method of Pressure-Phase Data Reduction
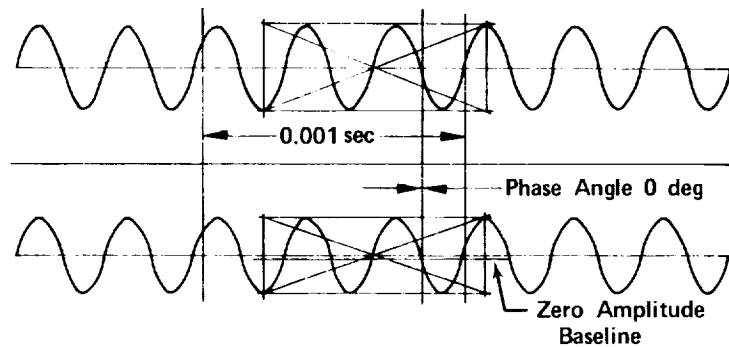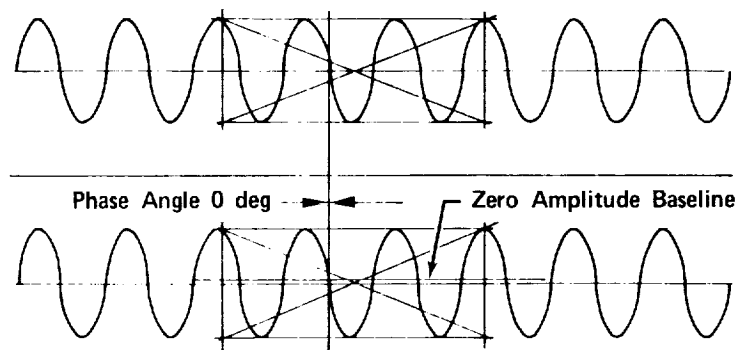
FD 37875

Figure III-20. Comparison of Typical Prerun and Postrun
Phase Shift Calibrations

a. Acoustic Resistance Data

Analysis of the acoustic resistance data was based on an attempt to verify the following equation for the specific acoustic resistance:

$$\theta = 0.37u/\sigma c C_f^2 \qquad (3)$$

where

θ = specific acoustic resistance

u = orifice particle velocity

σ = open area ratio

c = sonic velocity

C_f = flow coefficient of liner facing (see Appendix B).

To verify equation (3), it is necessary to show that the proportionality coefficient (0.37) was representative of the hot data. The value of this coefficient for all the acoustic resistance data was evaluated using the equation:

$$K = \frac{\theta \sigma c C_f^2}{u} \qquad (4)$$

The mean value of K for each liner test section and the cold flow data of Reference 1 are shown in figure III-21. The mean coefficients for the hot data do not significantly differ from the cold flow data, which may be substantiated by comparing the deviations as follows:

Type of Test	Average Deviation, %	Maximum Deviation, %
Cold Flow	12.5	32
Hot Firing	19.1	29

From these results, it was concluded that the acoustic resistance of partitioned liners operating under hot firing conditions can be described by the equation:

$$\theta = 0.37u/\sigma c C_f^2 \qquad (5)$$
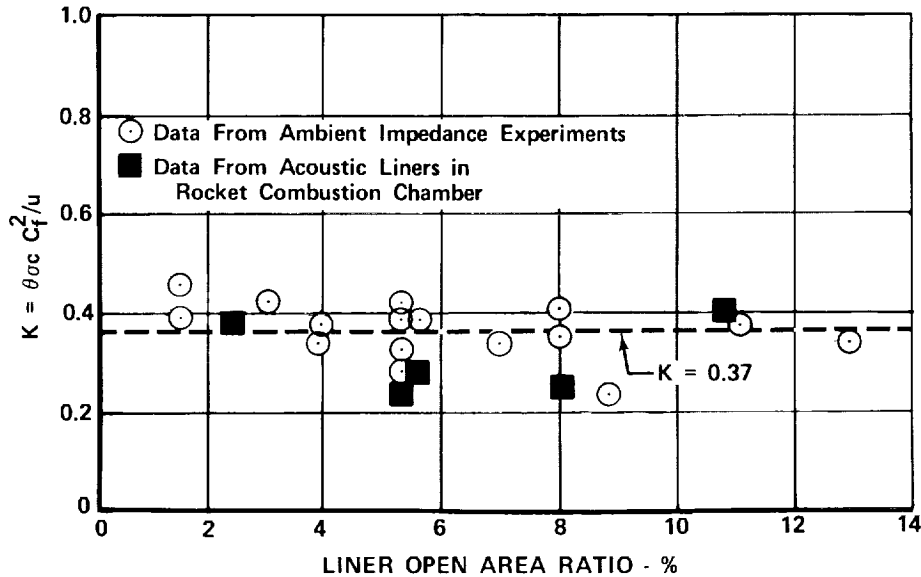
FD 37367A

Figure III-21. Comparison of Acoustic Resistance Data From
Ambient Impedance Experiments and Hot Firing
Rocket Tests

b. Acoustic Reactance Data

Using the data obtained from the high speed oscillographs, an analysis
was made to substantiate or improve the existing acoustic reactance theory.
The effective length of the apertures is the only empirical term in the
theory; therefore, the formula now in use for the effective length:

$$\ell_{T1} = T + D \qquad (6)$$

where T and D are the liner facing thickness and aperture diameter,
respectively, was compared to the experimental values. (See fig-
ure III-22.) The comparison showed that the theoretical effective
length was in error by 17%, on the average, and incorrect by as much
as 63% in individual cases. Thus, an investigation was made to find
a more suitable expression for the effective length. Because the
theoretical lengths computed using equation (6) were larger than the
experimental effective lengths, the equation:

$$\ell_{T2} = \sqrt{T^2 + D^2} \qquad (7)$$

was investigated. It was found that the error could be reduced to an
average of 12%; however, the values determined by equation (7) were
found to be smaller than the actual effective lengths. Finally, a third

III-29
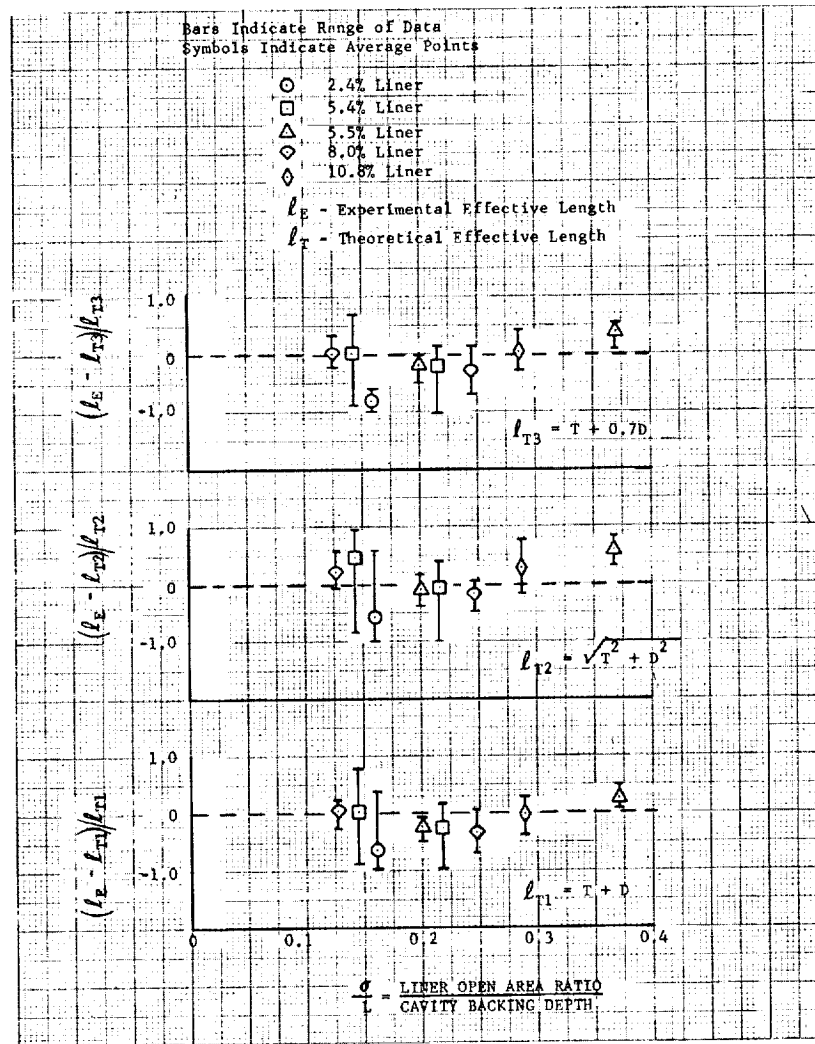
DF 79289

Figure III-22. Comparison of Experimental and Theoretical
Values of Effective Length

equation was used to predict the effective length that was shown to give the best fit to the hot data. This equation:

$$\ell_{T3} = T + 0.7D \qquad\qquad (8)$$

shows average agreement within 11% of the experimental data.

A comparison of the averaged experimental effective lengths from the ambient impedance experiments of Reference 1 and the Baseline Test Series was made with the theory of equation (8). The results are shown in figure III-23. The data from the ambient experiments fall, on the average, slightly higher than theory, and there is more scatter in the hot data; however, the theory is seen to be a fair representation of the entire data sample.

III-30

ℓ_{T3} - Theoretical Effective Length = T + 0.7D
ℓ_E - Experimental Data
T - Liner Thickness - in.
D - Aperture Diameter - in.

T/D = LINER THICKNESS/APERTURE DIAMETER

FD 37368C
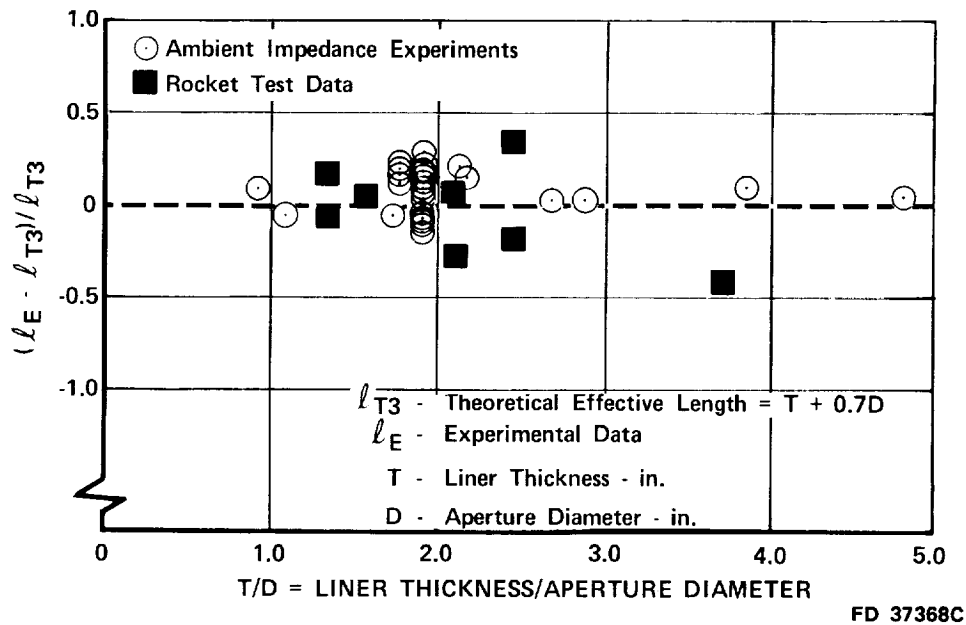
Figure III-23. Comparison of Aperture Effective Length Data
From Impedance Experiments and Hot Firing
Rocket Tests With Theory

c. Comparison of Absorption Coefficients

Analysis of the acoustic data computed from high-speed oscillograph
pressure-phase relations also included an evaluation of the accuracy of
the liner design theory in predicting the absorption coefficient for each
liner test section. To compute the theoretical absorption coefficients,
the theory outlined in Reference 1 was employed with the following exceptions:

1. The peak pressure amplitudes measured at the liner facing
   during the particular firing were used.

2. Effective aperture lengths were computed from equation (8).

3. No corrections were made to the theory to account for the
   chamber gas velocity.

4. Gas properties were based on the experimentally determined
   molecular weight of the cavity gases and the maximum recorded
   aperture gas temperatures.

5. Flow coefficients used were the experimentally determined
   values for the particular liner facing. (See Appendix B.)

A comparison of the experimental and theoretical absorption coefficients
is shown in figure III-24. Good agreement between theory and experiment
was obtained; the average deviation is only 11% for all liner test sections.
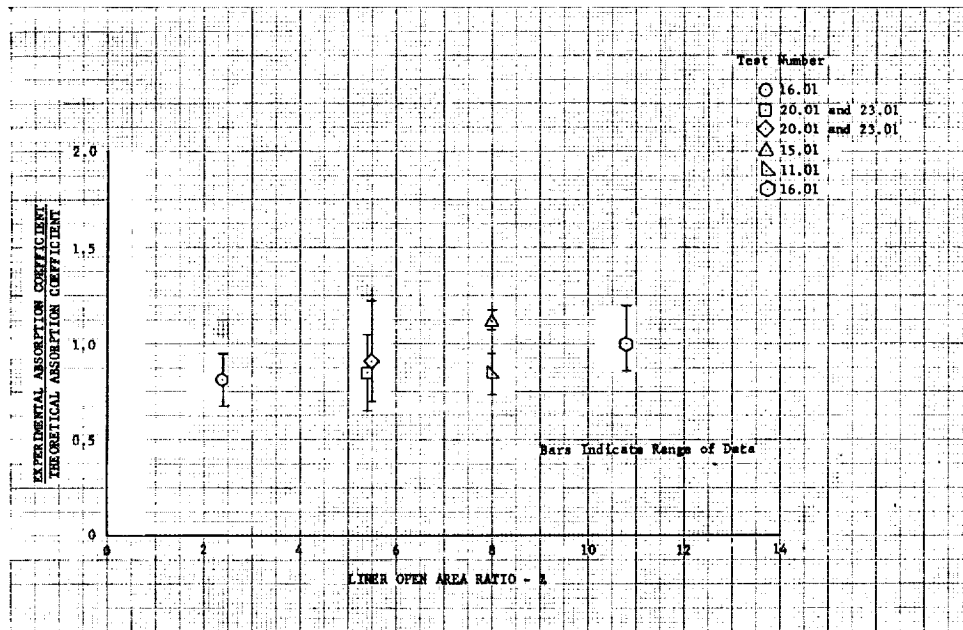
DF 79290

Figure III-24. Comparison of Experimental Absorption
Coefficients With Theory

SECTION IV
REFERENCES

1. "Suppression of Combustion Oscillations with Mechanical Damping Devices, Interim Report," Pratt & Whitney Aircraft, PWA FR-3299, August 1969.

2. Obert, C. L., and N. M. Kuluva, "Acoustic Liners for Large Engines, Final Report," R-7792, North American Rockwell Corp., Rocketdyne Div., March 1969.

3. "Suppression of Combustion Oscillations with Mechanical Damping Devices, Quarterly Progress Report No. 4," Pratt & Whitney Aircraft, PWA FR-3427, October 1969.

APPENDIX A

TEST DATA

Before preparing the high-speed oscillograph traces from which the pressure-phase data are obtained, a spectral analysis of the dynamic pressure data from each unstable test was performed. The analysis is necessary because the exact frequency of the predominant amplitudes must be known so that the data can be properly filtered before input to the oscillograph. The results of the spectral analysis are shown in figures A-1, A-2, and A-3. It was found that the peak-to-peak amplitudes in these figures are approximately 15% lower than those obtained from the oscillograph traces, a reduction caused by the narrow-band filtering and time-averaging techniques that were used to perform the spectral analysis. The inconsistency had no effect on the acoustic data, because all pressure amplitudes used in data reduction were taken from the oscillograph traces, not the above figures.

In table A-1, the pressure amplitudes, phase angles, and resulting liner acoustical properties for each unstable test are listed. A brief title describing the individual liner test section and the test number for which the data were obtained precedes each individual listing. Next, the properties of the gaseous medium and the dimensions of the resonator assembly that were input into the data reduction program are given. The following list identifies each heading:

DEN	Density (Aperture Gas), lb_m/ft^3
SONIC	Sonic Velocity (Aperture Gas), ft/sec
VIS	Dynamic Viscosity (Aperture Gas), $lb_m/ft/sec$
CF	Flow Coefficient
SIG	Open Area Ratio
XL	Cavity Backing Distance, in.
T	Liner Thickness, in.
D	Aperture Diameter, in.

Headings for the experimental data from the oscillograph traces and the resulting acoustical properties are:

Data

FREQ	Frequency, Hz
PA1	Chamber Pressure Amplitude Peak-to-Peak, $lb_f/in.^2$
PA2	Cavity Pressure Amplitude Peak-to-Peak, $lb_f/in.^2$
PHASE	Phase Angle, deg

Acoustical Properties

INERT	Specific Acoustic Inertance
REACT	Specific Acoustic Reactance
RESIS	Specific Acoustic Resistance
IMPED	Specific Acoustic Impedance
ABSOR	Absorption Coefficient
SPL	Incident Pressure Amplitude, db
UORF	Particle Velocity in Apertures, ft/sec
LEFF	Effective Length of Aperture, in.
K2RES	K_2 Resistance Proportionality Coefficient = RESIS σ cC_f^2/UORF

Chamber Pressures

Cavity Pressures
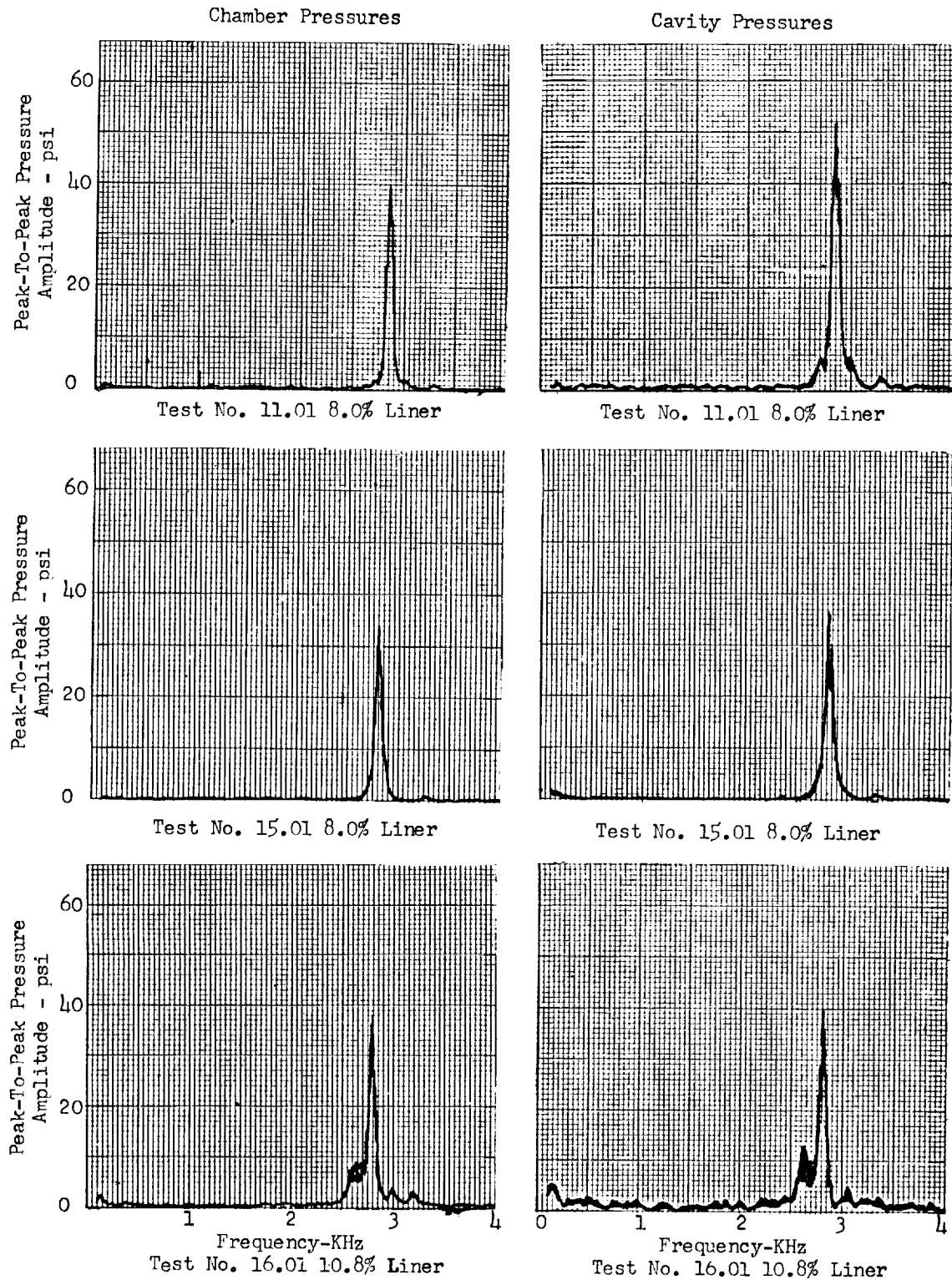
Figure A-1. Pressure Amplitude Data for Tests No. 11.01,
15.01, and 16.01

DF 78923

A-3

Chamber Pressures   Cavity Pressures

Test No. 16.01 2.4% Liner   Test No. 16.01 2.4% Liner

Test No. 20.01 5.5% Liner   Test No. 20.01 5.5% Liner

Test No. 20.01 5.4% Liner   Test No. 20.01 5.4% Liner
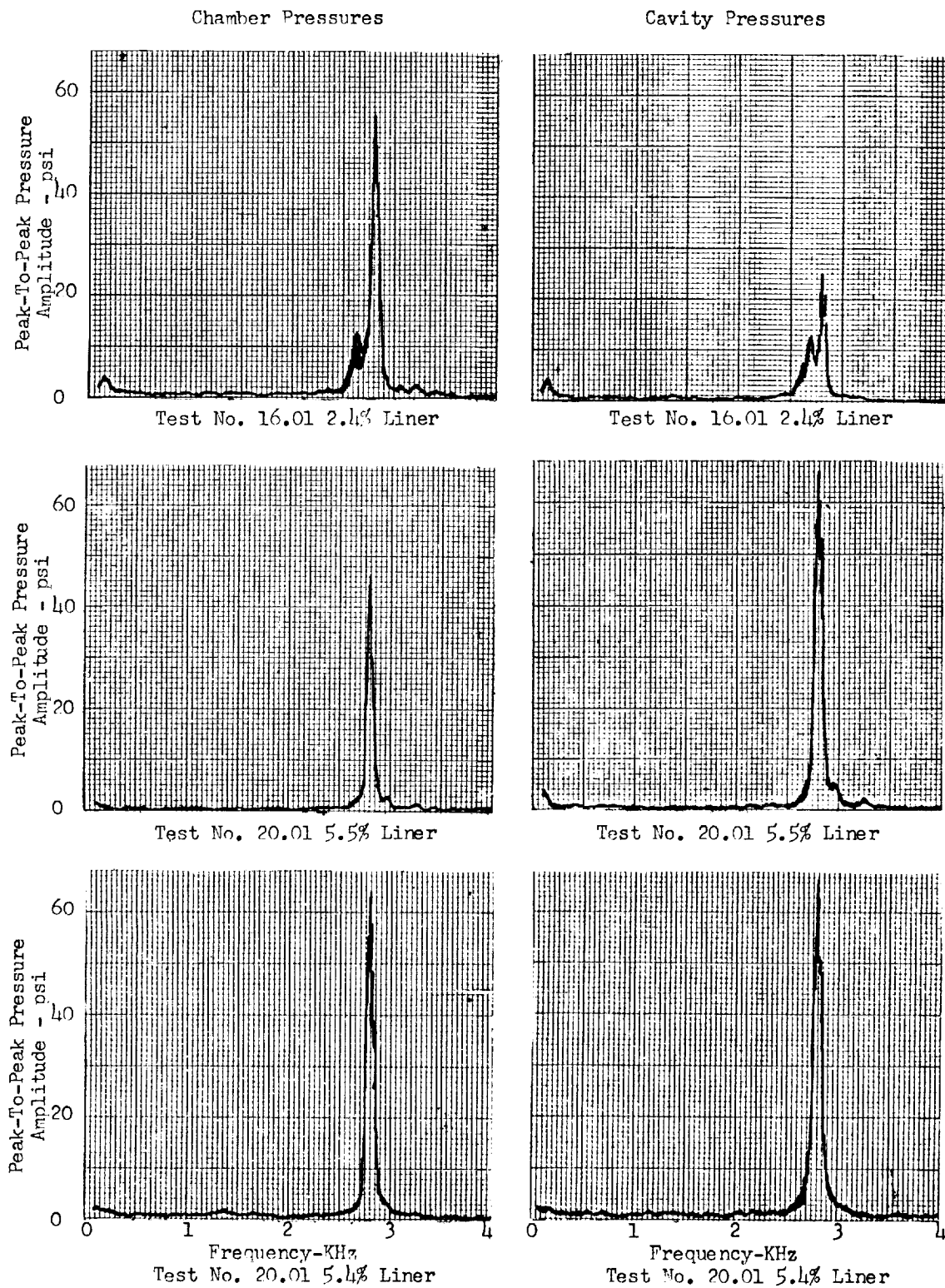
DF 78924

Figure A-2.   Pressure Amplitude Data for Tests No. 16.01
and 20.01

Chamber Pressures

Cavity Pressures

Test No. 23.01 5.5% Liner

Test No. 23.01 5.5% Liner

Test No. 23.01 5.4% Liner

Test No. 23.01 5.4% Liner
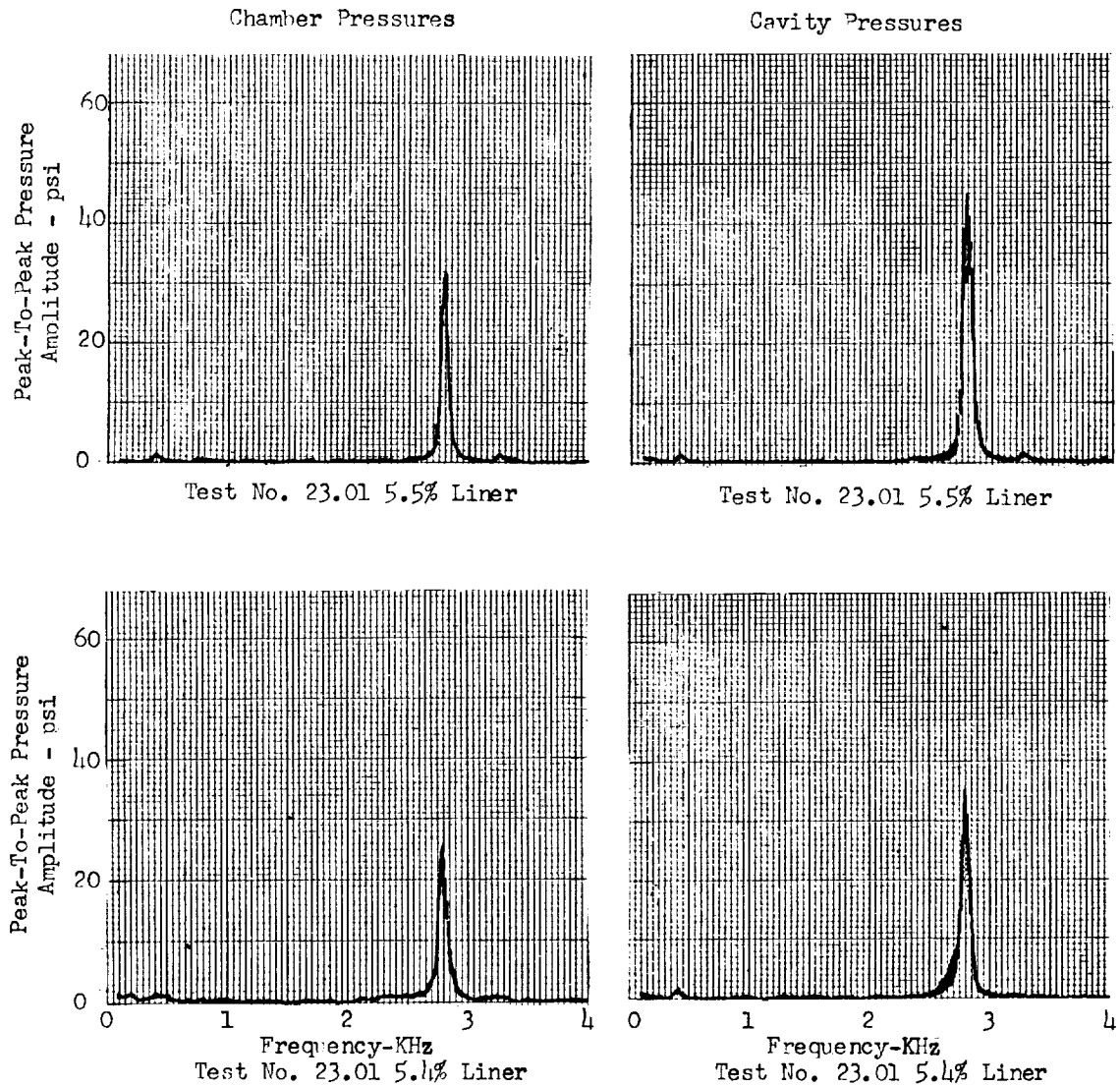
DF 78925

Figure A-3. Pressure Amplitude Data for Test No. 23.01

Table A-1. Acoustic Data From Hot Fire Tests

ACOUSTIC LINER TESTS HOT RUN 11.01 8.0 PERCENT LINER

DEN	SONIC	VIS	CF	SIG	XL	T	D
0.1000	2413.0	0.29000E-04	0.890	0.0800	0.325	0.200	0.096

FREQ	PA1	PA2	PHASE	INERT	REACT	RESIS	IMPED	ARSOR	SPL	UORF	LEFF	K2RES
2730.0	18.319	24.994	24.0	1.716	-3.477	1.548	3.80	0.333	187.81	1156.03	0.231	0.20
2730.0	18.319	24.994	40.0	2.278	-2.915	2.446	3.80	0.480	188.28	1156.03	0.307	0.32
2850.0	26.176	31.835	37.0	1.708	-3.267	2.462	4.09	0.434	191.22	1536.92	0.221	0.24
2850.0	26.176	31.835	41.0	1.987	-3.087	2.683	4.09	0.464	191.33	1536.92	0.244	0.26
2850.0	23.062	28.373	33.0	1.583	-3.391	2.202	4.04	0.404	190.03	1369.78	0.204	0.24
2850.0	23.062	28.373	21.0	1.199	-3.775	1.449	4.04	0.286	189.68	1369.78	0.155	0.16
2880.0	26.176	28.702	33.0	1.157	-3.765	1.445	4.49	0.375	191.04	1400.23	0.148	0.26
2880.0	26.176	28.702	37.0	1.337	-3.586	2.702	4.49	0.406	191.13	1400.23	0.171	0.29
2850.0	27.096	28.373	33.0	0.990	-3.984	2.587	4.75	0.360	191.29	1369.78	0.128	0.28
2850.0	27.096	28.373	41.0	1.390	-3.586	3.117	4.75	0.418	191.47	1369.78	0.179	0.34
2675.0	25.876	26.176	39.0	1.228	-4.072	2.297	5.24	0.376	190.94	1186.12	0.169	0.42
2675.0	25.876	26.176	27.0	0.631	-4.669	2.379	5.24	0.286	190.68	1186.12	0.087	0.30

ACOUSTIC LINER TESTS HOT RUN 15.01 8.0 PERCENT LINER

DEN	SONIC	VIS	CF	SIG	XL	T	D
0.0810	2650.0	0.29000E-04	0.889	0.0800	0.637	0.200	0.096

FREQ	PA1	PA2	PHASE	INERT	REACT	RESIS	IMPED	ARSOR	SPL	UORF	LEFF	K2RES
2000.0	22.160	21.554	67.5	1.660	-1.076	2.599	2.81	0.736	191.05	2127.35	0.231	0.20
2050.0	23.069	21.868	74.5	1.969	-0.815	2.942	3.05	0.726	191.67	2119.76	0.279	0.23
2050.0	23.386	20.982	66.1	1.527	-1.257	2.838	3.10	0.695	191.30	2033.93	0.217	0.23
2050.0	24.069	21.868	74.4	1.933	-0.851	3.051	3.16	0.712	191.92	2119.76	0.274	0.24
2050.0	26.945	22.789	70.6	1.679	-1.105	3.105	3.29	0.687	192.95	2208.95	0.268	0.23
2850.0	24.869	21.868	73.6	1.891	-0.894	3.039	3.16	0.710	191.91	2119.76	0.268	0.24
2800.0	25.802	20.982	84.0	2.470	-0.364	3.467	3.49	0.690	192.13	1998.25	0.357	0.29
2825.0	26.382	24.263	82.7	2.474	-0.335	3.037	3.05	0.740	192.59	2331.36	0.354	0.21
2800.0	23.676	27.169	72.9	1.945	-0.890	2.894	3.02	0.725	191.56	2111.30	0.281	0.22
2925.0	24.564	21.868	83.6	2.458	-0.351	3.137	3.15	0.727	191.90	2101.16	0.352	0.25
2875.0	23.676	21.868	69.6	1.749	-1.060	2.851	3.04	0.714	191.51	2101.16	0.250	0.22
2850.0	27.862	24.564	66.2	1.510	-1.275	2.890	3.15	0.689	192.79	2381.14	0.214	0.20

ACOUSTIC LINER TESTS HOT RUN 16.01 2.4 PERCENT LINER

DEN	SONIC	VIS	CF	SIG	XL	T	D
0.1000	2385.0	0.29000E-04	0.060	0.0240	0.150	0.250	0.067

FREQ	PA1	PA2	PHASE	IMFRT	RFACT	RESIS	IMPED	ARSOR	SPL	UORF	LEFF	K2RES
2830.0	33.335	20.554	53.0	0.257	-10.473	13.898	17.40	0.167	192.56	1551.74	0.009	0.47
2830.0	30.054	24.149	49.0	1.969	-8.761	10.078	13.35	0.202	191.75	1823.13	0.076	0.29
2830.0	30.054	24.149	53.0	2.603	-8.036	10.664	13.35	0.212	191.78	1823.13	0.104	0.30
2830.0	30.054	24.149	41.0	0.651	-10.078	9.761	13.35	0.179	191.69	1823.13	0.025	0.25
2900.0	37.936	24.998	58.0	2.146	-8.698	13.920	16.41	0.196	193.71	1867.19	0.083	0.39
2900.0	37.936	24.998	87.0	8.560	-2.284	16.255	16.41	0.214	193.78	1867.19	0.334	0.45
2900.0	37.936	24.998	90.0	10.845	-0.009	16.415	16.41	0.216	193.79	1867.19	0.423	0.46

Table A-1. Acoustic Data From Hot Fire Tests (Continued)

FREQ	PA1	PA2	PHASE	INERT	REACT	RESIS	IVPED	ABSOR	SPL	UORF	LEFF	K2RES
2850.0	34.112	26.176	45.0	0.036	-9.810	9.810	13.88	0.184	192.80	1990.10	0.032	0.26
2850.0	34.112	26.176	59.0	3.296	-7.359	11.775	13.88	0.216	192.89	1990.10	0.126	0.31
2850.0	34.112	25.176	42.0	0.335	-10.318	9.291	13.88	0.174	192.78	1990.10	0.012	0.24
2850.0	34.112	26.176	49.0	1.545	-9.100	10.479	13.89	0.195	192.83	1990.10	0.059	0.27

DEN	SONIC	VIS	CF	SIG	XL	T	
0.1100	2287.0	0.29000E-04	0.010	0.1080	0.375	0.150	0.094

ACOUSTIC LINER TESTS HOT RUN 15.01 10.8 PERCENT LINER

FREQ	PA1	PA2	PHASE	INERT	REACT	RESIS	IVPED	ABSOR	SPL	UORF	LEFF	K2RES
2850.0	27.096	28.373	49.0	1.522	-2.554	2.939	3.89	0.533	191.87	1190.02	0.251	0.50
2850.0	27.096	28.373	43.0	1.229	-2.948	2.944	3.89	0.494	191.73	1190.02	0.203	0.45
2830.0	27.727	30.054	33.0	0.929	-3.177	2.653	3.78	0.423	191.69	1251.69	0.154	0.33
2830.0	27.727	30.054	41.0	1.247	-2.859	2.485	3.78	0.488	191.91	1251.69	0.207	0.40
2830.0	27.727	30.054	43.0	1.335	-2.770	2.593	3.73	0.503	191.96	1251.59	0.222	0.42
2830.0	26.176	31.835	49.0	1.801	-2.216	2.548	3.37	0.582	191.77	1325.86	0.314	0.39
2830.0	26.176	31.835	37.0	1.400	-2.696	2.032	3.37	0.493	191.43	1325.86	0.234	0.31
2830.0	25.876	28.373	33.0	0.965	-3.141	2.039	3.74	0.427	191.10	1181.67	0.160	0.35
2830.0	25.876	28.373	45.0	1.458	-2.648	2.648	3.74	0.521	191.43	1181.67	0.242	0.45
2830.0	25.876	28.373	50.0	1.699	-2.407	2.869	3.74	0.552	191.55	1181.67	0.282	0.49
2830.0	27.096	30.402	33.0	1.037	-3.050	1.993	3.66	0.433	191.52	1266.19	0.172	0.32
2830.0	27.096	30.402	41.0	1.344	-2.762	2.401	3.66	0.500	191.75	1266.19	0.223	0.38
2830.0	27.096	30.402	49.0	1.705	-2.401	2.762	3.66	0.554	191.95	1266.19	0.283	0.44

DEN	SONIC	VIS	CF	SIG	XL	T	
0.0740	2776.0	0.29000E-04	0.016	0.0540	0.250	0.150	0.111

ACOUSTIC LINER TESTS HOT RUN 20.01 5.4 PERCENT LINER

FREQ	PA1	PA2	PHASE	INERT	REACT	RESIS	IVPED	ABSOR	SPL	UORF	LEFF	K2RES
2900.0	27.550	31.769	24.5	1.594	-5.975	2.723	6.56	0.219	191.04	1754.59	0.163	0.19
2925.0	32.701	40.790	33.1	2.464	-5.030	3.296	6.01	0.300	192.75	2272.92	0.249	0.18
2900.0	32.701	39.546	37.7	2.302	-5.268	3.382	6.26	0.288	192.71	2184.11	0.235	0.19
2925.0	32.082	35.976	33.1	1.898	-5.606	3.654	6.69	0.275	192.51	2004.64	0.192	0.22
2925.0	37.171	32.701	29.0	0.043	-7.460	4.135	8.53	0.201	193.60	1822.15	0.004	0.28

DEN	SONIC	VIS	CF	SIG	XL	T	
0.0869	2565.0	0.29000E-04	0.059	0.0550	0.150	0.250	0.101

ACOUSTIC LINER TESTS HOT RUN 20.01 5.5 PERCENT LINER

FREQ	PA1	PA2	PHASE	INERT	REACT	RESIS	IVPED	ABSOR	SPL	UORF	LEFF	K2RES
2900.0	17.693	24.263	20.0	3.676	-7.987	2.907	8.50	0.147	187.01	786.81	0.353	0.38
2925.0	27.262	38.637	28.3	4.378	-7.182	3.867	8.15	0.205	190.91	1264.10	0.417	0.31
2900.0	24.263	28.168	40.0	3.967	-7.696	6.458	10.04	0.224	189.95	913.42	0.381	0.73
2925.0	25.496	35.652	32.7	4.604	-6.952	4.463	9.22	0.228	190.39	1166.75	0.439	0.39
2900.0	20.168	38.340	41.4	5.235	-6.427	5.664	8.56	0.226	191.35	1243.25	0.504	0.47
2925.0	31.463	41.392	41.4	4.967	-6.593	5.812	8.70	0.259	192.30	1353.88	0.473	0.44
2925.0	27.550	36.590	41.5	5.040	-6.510	5.758	9.70	0.261	191.15	1197.37	0.481	0.50
2925.0	26.965	37.450	36.8	4.896	-6.663	4.945	9.32	0.248	190.93	1225.55	0.467	0.42

Table A-1. Acoustic Data From Hot Fire Tests (Continued)

ACOUSTIC LINER TESTS HOT RUN 23.01 5.4 PERCENT LINER

DEN	SONIC	VIS	CF	SIG	XL	T	D
0.0800	2672.0	0.290006E-04	0.920	0.0540	0.375	0.150	0.111

FREQ	DA1	DA2	PHASE	INERT	REACT	RESIS	IMPED	ABSOR	SPL	UORF	LEFF	K2RES
2850.0	13.737	22.537	66.0	3.501	-1.183	2.658	2.91	0.719	186.80	1896.04	0.347	0.17
2850.0	13.737	19.404	74.0	3.843	-0.931	3.249	3.38	0.686	186.63	1632.48	0.371	0.24
2820.0	21.523	16.001	66.0	2.326	-2.490	5.614	6.14	0.449	189.57	1406.86	0.227	0.48
2820.0	21.523	16.001	43.0	0.331	-4.494	4.191	6.14	0.355	189.28	1406.86	0.032	0.36
2850.0	24.712	18.531	49.0	0.597	-4.177	4.805	6.36	0.375	190.54	1559.00	0.057	0.37
2830.0	16.516	21.523	66.0	2.307	-1.500	3.370	3.68	0.661	187.97	1798.00	0.322	0.22
2830.0	16.516	21.523	79.0	4.041	-0.767	3.609	3.68	0.661	188.11	1798.00	0.393	0.24
2830.0	15.592	21.033	60.0	3.026	-1.782	3.087	3.56	0.621	197.43	1757.07	0.294	0.21
2830.0	15.592	21.033	98.0	4.684	-0.124	3.562	3.56	0.694	187.43	1757.07	0.456	0.24
2820.0	15.592	21.033	90.0	4.808	-0.000	3.564	3.56	0.684	187.72	1757.07	0.468	0.24
2820.0	15.592	21.033	67.0	3.135	-1.673	3.147	3.56	0.629	187.47	1757.07	0.305	0.21
2820.0	22.537	15.592	55.0	0.924	-4.000	5.713	6.97	0.374	189.73	1297.93	0.080	0.53
2820.0	22.537	15.592	55.0	0.824	-4.000	5.713	6.97	0.374	189.73	1297.93	0.080	0.53
2820.0	14.395	14.395	50.0	7.340	-2.485	4.136	4.82	0.508	186.28	1197.43	0.228	0.42
2820.0	14.385	14.385	74.0	3.495	-1.330	4.638	4.82	0.552	186.45	1197.43	0.341	0.47
2820.0	14.385	14.385	62.0	2.560	-2.265	4.260	4.82	0.519	186.32	1197.43	0.250	0.43

ACOUSTIC LINER TESTS HOT RUN 23.01 5.5 PERCENT LINER

DEN	SONIC	VIS	CF	SIG	XL	T	D
0.0800	2565.0	0.290006E-04	0.960	0.0550	0.275	0.250	0.101

FREQ	DA1	DA2	PHASE	INERT	REACT	RESIS	IMPED	ABSOR	SPL	UORF	LEFF	K2RES
2770.0	19.319	24.712	47.0	3.179	-3.251	3.486	4.76	0.454	188.19	1403.33	0.309	0.25
2800.0	17.294	25.287	45.0	3.285	-3.076	3.075	4.35	0.471	187.75	1451.57	0.316	0.22
2820.0	19.100	25.676	42.0	3.031	-3.285	2.958	4.42	0.447	188.07	1495.99	0.289	0.20
2850.0	16.327	23.320	45.0	3.157	-3.093	3.093	4.37	0.470	187.24	1363.09	0.298	0.23
2850.0	16.327	23.329	41.0	2.949	-3.301	2.869	4.37	0.443	187.15	1363.09	0.278	0.21
2850.0	16.327	23.320	37.0	2.756	-3.493	2.637	4.37	0.414	187.06	1363.09	0.260	0.20
2760.0	20.554	27.096	40.0	2.447	-3.803	3.191	4.96	0.399	189.01	1511.91	0.231	0.22
2760.0	22.798	27.096	45.0	2.614	-3.840	3.840	5.43	0.402	189.92	1533.17	0.255	0.26
2740.0	22.798	27.096	31.0	1.799	-4.654	7.796	5.43	0.310	189.64	1533.17	0.175	0.19
2770.0	22.798	27.287	23.0	1.892	-4.538	2.947	5.43	0.325	189.69	1538.72	0.184	0.17
2720.0	17.794	25.287	33.0	2.712	-3.649	7.369	4.35	0.394	187.46	1451.57	0.261	0.17
2840.0	19.310	25.580	37.0	2.677	-3.577	2.695	4.47	0.407	188.04	1493.55	0.253	0.18
2840.0	19.310	25.580	51.0	3.435	-2.818	2.695	4.47	0.407	188.04	1493.55	0.253	0.18
2840.0	19.310	25.580	45.0	3.087	-3.167	3.491	4.47	0.495	188.34	1493.55	0.325	0.24
2850.0	20.702	27.410	41.0	2.672	-3.578	3.167	4.74	0.462	188.22	1601.50	0.292	0.22
2850.0	20.702	27.410	33.0	2.273	-3.976	3.110	4.74	0.418	189.17	1601.50	0.252	0.20
2850.0	21.033	27.096	36.0	2.325	-3.925	2.582	4.85	0.360	188.99	1593.16	0.215	0.16
2850.0	21.033	27.096	50.0	3.131	-3.119	2.851	4.85	0.377	189.14	1583.16	0.219	0.18
						3.716		0.464	189.43		0.296	0.24

A-8

APPENDIX B
APERTURE FLOW COEFFICIENT EXPERIMENTS

Steady-state flow tests of the Task I resonator elements were con-
ducted to determine the flow coefficients of the aperture arrays. The
test apparatus (figure B-1) consisted of a flow orifice through which
gaseous nitrogen flowed into a manifold tube mounted in place of the
rear cavity wall of the liner test sections. In the experiments, the
gas supply was set to produce various velocities in the liner apertures
so that Reynolds numbers from $0.4 \times 10^{+6}$ to $2.0 \times 10^{+6}$ could be obtained;
this range corresponded to the expected Reynolds numbers produced by
the oscillatory velocities in the liner apertures during the hot tests.
The flow coefficient was determined from the equation

$$C_f = \frac{w}{0.525\ Y_1 D_2 \sqrt{\rho \Delta P}}$$

where

w = flowrate (lb_m/sec)

D_2 = effective diameter of the apertures

ρ = upstream density (lb_m/ft^3)

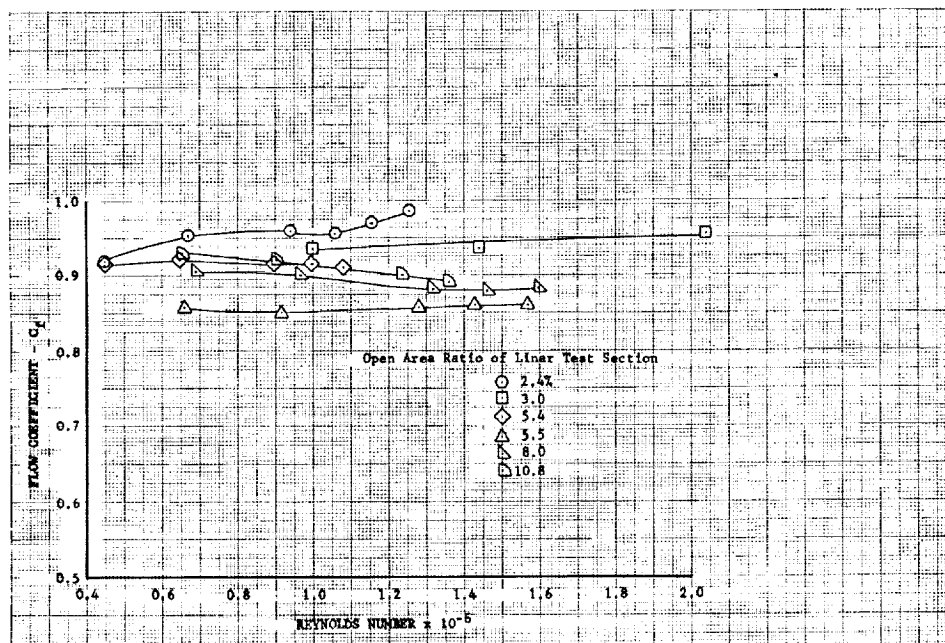ΔP = pressure differential across the apertures (psid)

Y_1 = compressibility factor.

Results of the experiments (figure B-2) were used in the analysis of
the acoustic data obtained from the test series.
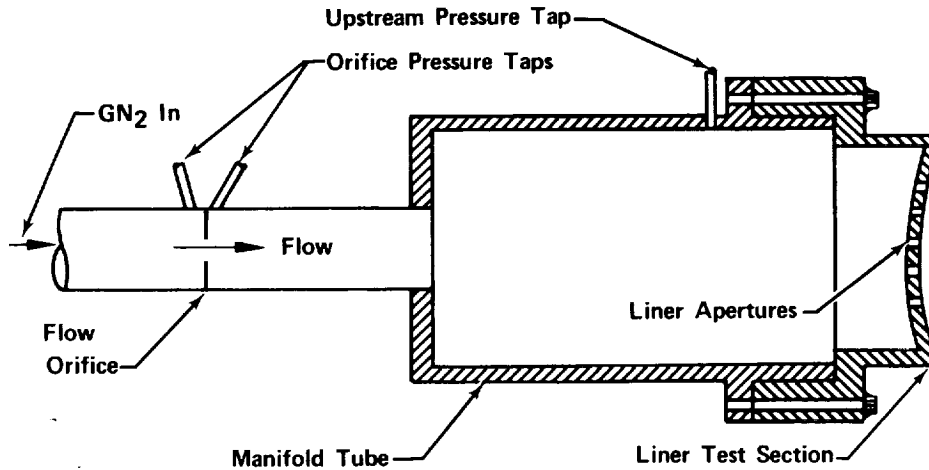
FD 36172

Figure B-1. Apparatus Used to Determine Flow Coefficients
of Liner Samples

DF 79291

Figure B-2. Flow Coefficients of Liner Test Sections

APPENDIX C
DISTRIBUTION LIST*

Copies	Recipient	Designee

NASA
Marshall Space Flight Center
Huntsville, Alabama 35812

2   Office of Technical Information,
       A&TS-MS-IP

1   Technical Library, A&TS-MS-IL

1   Purchasing Office, A&TS-PR-MBB

1   Patent Office, A&TS-PAT

1   Mr. Dale Burrows, S&E-ASTN-PJ

1   Technology Utilization Office, A&TS-TU

3   Mr. Richard H. Counts, S&E-ASTN-PPB

1   Mr. Rex Bailey, S&E-ASTN-PPB

1   Mr. Robert J. Richmond, S&E-ASTN-PP

3   Chief, Liquid Propulsion Experimental Engineering, RPX
     NASA Headquarters
     Washington, D. C. 20546

3   Chief, Liquid Propulsion Technology, RPL
     Office of Advanced Research and Technology
     NASA Headquarters
     Washington, D. C. 20546

24   NASA Scientific and Technical Information Facility
     P. O. Box 33
     College Park, Maryland 20740

1   Director, Launch Vehicles and Propulsion, SV
     Office of Space Science and Applications
     NASA Headquarters,
     Washington, D. C. 20546

1   Mr. Charles Donlan
     Director, Advanced Manned Missions, MT
     Office of Manned Space Flight
     NASA Headquarters,
     Washington, D. C. 20546

1   Mr. Leonard Roberts
     Mission Analysis Division
     NASA Ames Research Center
     Moffett Field, California 94035

---

* This report has been sent directly to the "recipient" except where the
technical librarian for the recipient is designated. In these cases,
the report has been sent to the librarian and a copy of the transmittal
letter to the recipient.

Copies	Recipient	Designee
1	Mr. K. R. Collins, Assistant Program Manager Bldg. 2025, Dept 9800 Aerojet Liquid Rocket Company P. O. Box 13222 Sacramento, California 95813	
1	Mr. James E. Hale, Project Engineer Mail Code AA72 Rocketdyne, North American Rockwell Corporation 6633 Canoga Avenue Canoga Park, California 91304	
1	Mr. William Creslein P. O. Box 2691 - FRDC Pratt & Whitney Aircraft Division United Aircraft Corporation West Palm Beach, Florida 33402	
1	Jerry Thomson Code PD-RV George C. Marshall Space Flight Center Marshall Space Flight Center, Alabama 35812	
1	NASA Ames Research Center Moffett Field, California 90435	Mr. H. J. Allen
1	NASA Goddard Space Flight Center Greenbelt, Maryland 20771	Mr. Merland L. Moseson Code 620
1	NASA Jet Propulsion Laboratory California Institute of Technology 4800 Oak Grove Drive Pasadena, California 91103	Mr. Henry Burlage, Jr. Propulsion Div 38
1	NASA Langley Research Center Langley Station Hampton, Virginia 23365	Mr. Ed Cortwright Director
2	NASA Lewis Research Center 21000 Brookpark Road Cleveland, Ohio 44135	Dr. Bruce T. Lundin Director Dr. Richard Priem
1	NASA Marshall Space Flight Center Marshall Space Flight Center, Alabama 35812	Mr. Hans G. Paul S&E-ASTN-P
2	NASA Manned Spacecraft Center Houston, Texas 77001	Dr. Robert Gilruth Director Mr. Cecil Gibson Code EP2
1	NASA John F. Kennedy Space Center Kennedy Space Center, Florida 32899	Dr. K. H. Debus Director

Copies	Recipient	Designee
1	Aeronautical Systems Division Air Force Systems Command Wright-Patterson Air Force Base Dayton, Ohio 45433	Mr. D. L. Schmidt Code ASRCNC-2
1	Commander, Office of Research Analyses (OAR) Holloman Air Force Base, New Mexico 88330 Attn: RRRD	Librarian
1	Air Force Missile Test Center Patrick Air Force Base, Florida	Mr. L. J. Ullian
1	Space & Missile Systems Organization Los Angeles 45, California	Col. Clark Technical Data Center
1	Arnold Engineering Development Center Arnold Air Force Station Tullahoma, Tennessee	Dr. H. K. Doetsch
1	Bureau of Naval Weapons Department of the Navy Washington, D. C.	Mr. J. Kay RTMS-41
1	Defense Documentation Center Headquarters Cameron Station, Building 5 5010 Duke Street Alexandria, Virginia 22314	TISIA
1	Headquarters, U. S. Air Force Washington 25, D. C.	Col. C. K. Stambaugh AFRST
1	Picatinny Arsenal Dover, New Jersey 07801	Mr. I. Forsten, Chief Liquid Propulsion Laboratory, SMUPA-DL
2	Air Force Rocket Propulsion Laboratory Research and Technology Division Air Force System Command Edwards, California 93523	RPS Mr. H. Main RPRRG/Lt. W. Pritz
1	U. S. Army Missile Command Redstone Arsenal Alabama 35809	Dr. Walter Wharton
1	U. S. Naval Ordnance Test Station China Lake California 93557	Code 4562 Chief, Missile Propulsion Div.
1	Chemical Propulsion Information Agency Applied Physics Laboratory 8621 Georgia Avenue Silver Spring, Maryland 20910	Mr. Tom Reedy

Copies	Recipient	Designee
1	Aerojet-General Corporation P. O. Box 1947 Technical Library, Bldg 2015, Dept 2410 Sacramento, California 95809	Mr. R. Stiff
1	Aeronutronic Philco Ford Corporation Ford Road Newport Beach, California 92663	Librarian
1	Aerospace Corporation 2400 East El Segundo Boulevard P. O. Box 95085 Los Angeles, California 90045	Mr. John G. Wilder MS-2293 Propulsion Dept
1	Arthur D. Little, Inc. 20 Acorn Park Cambridge, Massachusetts 02140	Library
1	Astropower Laboratory Douglas Aircraft Company 2121 Campus Drive Newport Beach, California 92663	Dr. Goerge Moe Director
1	Atlantic Research Corporation Edsall Road and Shirley Highway Alexandria, Virginia 22314	Librarian
1	Beech Aircraft Corporation Boulder Division Box 631 Boulder, Colorado	Mr. J. H. Rodgers
1	Bell Aerosystems Company P. O. Box 1 Buffalo, New York 14240	Mr. W. M. Smith
1	BellComm 1100 17th Street Washington, D. C.	Library
1	Bendix Systems Division Bendix Corporation 3300 Plymouth Road Ann Arbor, Michigan	Mr. John M. Brueger
1	The Boeing Company P. O. Box 3707 Seattle, Washington 98124	Library
1	The Boeing Company P. O. Box 1680 Huntsville, Alabama 35801	Mr. Ted Snow

Copies	Recipient	Designee
1	Missile Division Chrysler Corporation P. O. Box 2628 Detroit, Michigan 48231	Mr. John Gates
1	Wright Aeronautical Division Curtiss-Wright Corporation Wood-Ridge, New Jersey 07075	Mr. G. Kelly
1	Missile and Space Systems Division McDonnell Douglas Aircraft Corporation 5301 Bolsa Avenue Huntington Beach, California 92647	Mr. R. W. Hallet Chief Engineer Advanced Space Tech.
1	Aircraft Missiles Division Fairchild Hiller Corporation Hagerstown, Maryland 21740	Librarian
1	General Dynamics/Convair Library and Information Services, Department 128-00 San Diego, California 92112	Mr. Frank Dore
1	Re-Entry Systems Department General Electric Company 3198 Chestnut Street Philadelphia, Pennsylvania 19101	Mr. F. E. Schultz
1	Advanced Engine & Technology Department General Electric Company Cincinnati, Ohio 45215	Mr. D. Suichu
1	Grumman Aircraft Engineering Corporation Bethpage, Long Island New York	Mr. Joseph Gavin
1	Ling-Temco-Vought Corporation Astronautics Division P. O. Box 5907 Dallas, Texas 75222	Librarian
1	Lockheed Propulsion Company P. O. Box 111 Redlands, California 92374	Mr. H. L. Thackwell
1	Lockheed Missiles and Space Co. Attn: Technical Information Center P. O. Box 504 Sunnyvale, California 94088	Librarian
1	The Marquardt Corporation 16555 Saticoy Street Van Nuys, California 91409	Mr. Leo Bell

Copies	Recipient	Designee
1	Denver Division Martin Marietta Corporation P. O. Box 179 Denver, Colorado 80201	Dr. Morganthaler
1	McDonnell Douglas Aircraft Corporation P. O. Box 516 Municipal Airport St. Louis, Missouri 63166	Mr. R. A. Herzmark
1	Space Division North American Rockwell, Inc 12214 Lakewood Boulevard Downey, California 90241	Library
1	Rocketdyne (Library 586- 306) 6633 Canoga Avenue Canoga Park, California 91304	Dr. R. I. Thompson
1	Northrop Space Laboratories 3401 West Broadway Hawthorne, California	Dr. William Howard
1	Astro-Electronics Division Radio Corporation of America Princeton, New Jersey 08540	Librarian
1	Space General Corporation 9200 East Flair Avenue El Monte, California 91734	Librarian
1	Stanford Research Institute 333 Ravenswood Avenue Menlo Park, California 94025	Dr. Gerald Marksman
1	TRW Systems Group TRW, Incorporated One Space Park Redondo Beach, California 90278	Mr. G. W. Elverum
1	TAPCO Division TRW, Incorporated 23555 Euclid Avenue Cleveland, Ohio 44117	Mr. P. T. Angell
1	Thiokol Chemical Corporation Huntsville Division Huntsville, Alabama	Mr. John Goodloe
1	United Aircraft Corporation 400 Main Street East Hartford, Connecticut 06108	Librarian

Copies	Recipient	Designee
1	United Technology Center 587 Methilda Avenue P. O. Box 358 Sunnyvale, California 94088	Dr. David Altman
1	Aerospace Operations Walter Kidde and Company, Inc. 567 Main Street Belleville, New Jersey 07109	Mr. R. J. Hanville
1	Rocket Research Corporation 11441 Willow Road Redmond, Washington 98052	Mr. Foy McCullough, Jr.
1	The Johns Hopkins University Applied Physics Laboratory 8621 Georgia Avenue Silver Spring, Maryland 20910	Dr. W. G. Berl
1	Ohio State University Rocket Research Laboratory Department of Aeronautical and Astronautical Engineering Columbus, Ohio 43201	Dr. R. Edse
2	Princeton University Forrestal Research Center Princeton, New Jersey 08540	Dr. I. Glassman Mr. D. T. Harje
1	University of Wisconsin Dept. of Mechanical Engineering Madison, Wisconsin 53705	Dr. P. S. Myers
1	University of Michigan Aeronautical & Astronautical Engineering Laboratories Aircraft Propulsion Lab North Campus Ann Arbor, Michigan 48105	Dr. J. A. Nicholls
1	Institute of Engineering Research University of California Berkeley, California 94720	Dr. A. K. Oppenheim
1	Purdue University School of Mechanical Engineering Lafayette, Indiana 46207	Dr. J. R. Osborn
1	Massachusetts Institute of Technology Department of Mechanical Engineering Cambridge, Massachusetts 02139	Dr. T. Y. Toong
1	Illinois Institute of Technology 10 W. 35th Street Chicago, Illinois 60616	Dr. P. T. Torda

Copies	Recipient	Designee
1	Georgia Institute of Technology Aerospace School Atlanta, Georgia 30332	Dr. Ben T. Zinn
1	The Pennsylvania State University Mechanical Engineering Department 207 Mechanical Engineering Boulevard University Park, Pennsylvania 16502	Mr. G. M. Faeth